Universidade do Minho
Escola de Engenharia

Samuel Araújo Silva

Development of an electrochemical sensor for detection of organic water contaminants (Atrazine) based on molecular imprinted polymers

Master thesis
Integrated Master in Biological Engineering

Supervisors:

João Monteiro Peixoto
Raquel Barbosa Queirós

February 2021

Universidade do Minho
Escola de Engenharia

Samuel Araújo Silva

Development of an electrochemical sensor for detection of organic water contaminants (Atrazine) based on molecular imprinted polymers

Master thesis
Integrated Master in Biological Engineering

Supervisors:

João Monteiro Peixoto
Raquel Barbosa Queirós

February 2021

GRATEFUL/AGRADECIMENTOS

Esta tese é dedicada aos meus pais, Carlos Silva e Odete Araújo, por todo apoio dado que me permitiu chegar onde estou hoje. É com todo o meu afeto que vos agradeço por todos os vossos sacrifícios.

Quero agradecer ao meu irmão, Leandro, que me emprestou o rato para a realização desta tese. O que me facilitou bastante o trabalho escrito. Sei que poderei sempre contar com o teu apoio, meu irmão!

À minha namorada, Catarina Pinto, que sempre me apoiou e me aconselhou pelo melhor.

Aos meus amigos, grandes companheiros, que estiveram ao meu lado e me apoiaram durante o meu percurso académico e durante a minha dissertação.

À minha orientadora, doutora Raquel Queirós, que me ajudou desde o início, que me transmitiu novos conhecimentos e esteve sempre disponível para me ajudar na realização desta dissertação. Quero agradecer o seu apoio e confiança. Quero também apresentar os meus sentimentos, pelo material laboratorial partido.

Ao Water Quality Group, pela oportunidade de trabalhar junto deles, por me terem ajudado sempre que precisei, pelo apoio e tempo prestado.

Ao doutor Álvaro Geraldes, que me ajudou e orientou na elaboração do software descrito neste trabalho.

Por fim, o meu agradecimento especial ao meu orientador académico, professor João Peixoto, que me honrou com o seu apoio.

STATEMENT OF INTEGRITY

I hereby declare having conducted this academic work with integrity. I confirm that I have not used plagiarism or any form of undue use of information or falsification of results along the process leading to its elaboration.

I further declare that I have fully acknowledged the Code of Ethical Conduct of the University of Minho.

Abstract

Chemical pollution of surface waters poses a threat to the aquatic environment, with acute and chronic toxicity effects to the aquatic organisms, loss of habitats and biodiversity, and that pose a threat to human health. European Union Directive 2013/39/EU establishing a framework for community action which involves the identification of substances which take priority over those which constitute a significant risk to or via the aquatic environment at Union level (EC, 2013).

On this work, an electrochemical sensor based on Molecular Imprinted Polymers (MIPs) for the detection of atrazine (ATZ) was developed. The MIP was successfully electropolymerized onto the surface of a gold microfabricated electrode. A calibration curve for different ATZ concentrations in water samples was calculated and a dynamic range between 0 to 25 μg/L and a LOD of 1.63 μg/L were found. The results obtained from the characterization techniques, atomic force microscopy and scanning electron microscopy showed concordant and consistent results with the electrochemical measurements that can be associated with the formation of a polymer layer at the electrode surface. However, according to the current results further optimization and study is required, especially for the extraction of ATZ from the MIP.

Keywords

MIP, Electrochemical sensor, Electropolymerization, Microfabricated gold electrode.

Resumo

A poluição química das águas superficiais representa uma ameaça ao ambiente aquático com efeitos de toxicidade aguda e crônica para os organismos aquáticos, perda de habitats e biodiversidade, e que representa uma ameaça para a saúde humana. A Diretiva da União Europeia 2013/39/EU que estabelece um quadro de ação comunitária que envolve a identificação de substâncias prioritárias em relação às que constituem um risco significativo para ou através do ambiente aquático a nível da União Europeia (EC, 2013).

Neste trabalho, um sensor eletroquímico baseado em polímeros molecularmente impressos para a deteção de atrazina foi desenvolvido. O polímero molecularmente impresso foi eletropolimerizado com sucesso na superfície de um elétrodo de ouro. A curva de calibração para diferentes concentrações de atrazina em água foi calculada com uma faixa dinâmica entre 0 µg/L a 25 µg/L e um limite de deteção de 1,63 µg/L. Os resultados obtidos da caracterização por microscopia de força atómica e de varrimento de eletrões mostram resultados concordantes e que validam a formação de um filme de polímero na superfície do elétrodo. Não obstante, são necessários mais estudos e otimização, especialmente da etapa de extração do analíto da matriz do polímero

Palavras-Chave

Polímeros molecularmente impressos, Sensores eletroquímicos, Electropolimerização, Elétrodos microfabricados

INDEX

FIGURE INDEX

TABLE INDEX

1. INTRODUCTION

Water is a resource essential to life. It sustains all forms of ecosystems; aquatic environments, detained more biodiversity than any other one and since is one of the most precious resource in the planet needs to be protected. Unfortunately, water contamination is growing, threatening and destroying habitats, reducing biodiversity and contaminating all source of species. Agriculture is on top ranking in what concerns soil and water contamination, a growing industry in demand, henceforth the technology and strategies behind it need to become more efficient in order to achieve a higher productivity, and the use of pesticides, herbicides and fertilizers is increasing to achieve the rising goal. Residuals from agriculture are very common and constitute a source of water contamination by herbicides and pesticides. They are easily eluted from the grow to surface water and underground water, increasing toxicity levels in aquatic organisms, that by their turn threat the health of the communities in the higher levels of the food chain, including us. Such contaminates accumulation represent a significant danger to aquatic environments and all living beings. One of the most used herbicides in the world is atrazine (ATZ), whose introduction in agriculture relates to 1958.

However, European Parliament poses Directives for the establishing of frameworks for Community actions and defines a list of priority substances (see annex A) with a high risk associated (EC, 2013), that should be identified and quantified in surface waters. One of the chemical species mentioned is ATZ, it's an herbicide with a slow degradation of few months on soil and even slower on water (Moreira et al., 2017), it is often found in groundwater in USA and in Europe (Ackerman, 2007). This molecule has been suspected since 2000 to have negative impacts in the human reproductive system and was also studied against effects on the brain (Rodriguez et al., 2005). Furthermore, traditional methods for detection of ATZ are not reliable as they are expensive, time consuming and can't be applied in real time detection, such as high-performance liquid chromatography, enzyme linked immunosorbent assay and gas chromatography. This topic is better discussed in section 1.3.

1.1 Atrazine Metabolites

ATZ is an herbicide that belongs to a class of heterocycles containing nitrogen molecules, also called triazines. It has a ring structure containing nitrogen with the chemical formula $C_8H_{14}ClN_5$ (see figure 1). This chemical compound is stable when in slightly acid or basic mediums. It doesn't occur naturally in the wild, it's synthetized by reacting cyanuric chloride with isopropylamine forming dichloro-6-

isopropylamino-s-triazine and by its turn is reacted with monoethylamine and diluted caustic. Also, this herbicide is available in different forms such as powder, granules and liquid formulations (WHO, 1991).

Whenever present in soil, ATZ can be biodegraded by several bacteria, an article dating 1997 explains the pathways and the metabolites formed in the biodegradation process of ATZ. One of the pathways relates to ATZ hydrolysation by *Pseudomonas sp*. into hydroxyatrazine, a nontoxic metabolite, that by its turn can be catalysed into N-isopropylammelide by hydrolyzation of the ethylamino group (N-CH_2CH_3) of the hydroxyatrazine. Nevertheless, ATZ biodegradation can also follow a second pathway by *Rhodococcus*, through the dealkylation of the alkyl group (N-CH_2) present in the molecule, forming deisopropylatrazine (DIA) and deethylatrazine, often referred as DEA (Boundy-Mills et al., 1997). Both the hydrolyzation and the dealkylation pathways, are illustrated in figure 1.

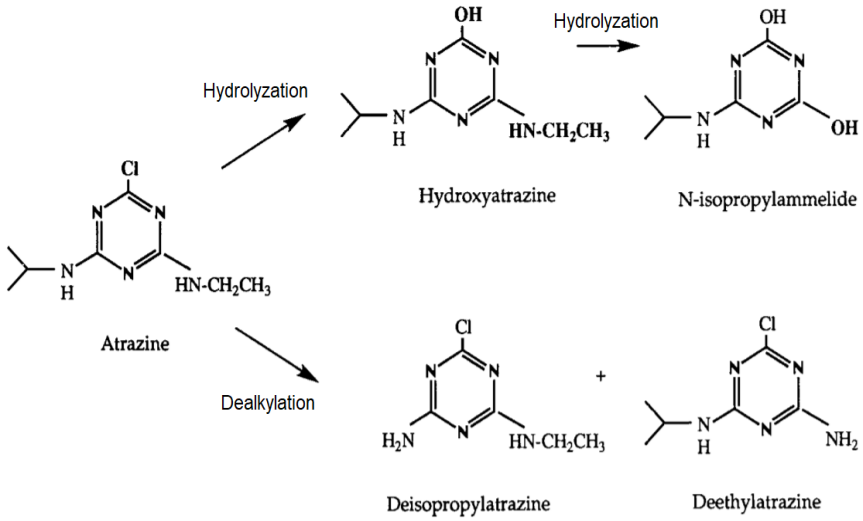

Figure 1. Atrazine degradation pathways in soil, adapted from (Kyria L. Boundy-Mills, 1997).

1.2 Atrazine Impacts

ATZ is very unstable when present on soil, but when in water ATZ is more stable and thus a big treat for the ecosystems, since it affects the communities and changes the water quality. One of the first indicators of ATZ in aquatic ecosystems, is the reduction in dissolved oxygen and the possible increase in water turbidity. Algal and plants communities, such as phytoplankton and macrophytes, are directly affect by photosynthesis inhibition, reducing biomass levels and productivity in the ecosystem, this impact indirectly disturbs the heterotrophic species in the higher levels of the food chain. Additionally, many

zooplankton communities and aquatic insects, show reduced growth and reproduction levels when exposed to ATZ concentrations, ranging from 20 µg/L up to 500 µg/L. Other invertebrates and herbicides are affected by the lost on aquatic plants communities. Vertebrate species, like mammals and fishes are even more sensitive to ATZ, concentrations as low as 3µg/L have major impact in those living beings. On their turn, fish growth, behaviour and physiology changes are common in many species, ATZ is metabolised in the kidneys of those animals and excreted through the gills; thus, some species may present altered tissues in those areas (Graymore et al., 2001). All things considered, ATZ affects abiotic and biotic parameters of ecosystems, it directly reduces growth and productivity of autotrophic communities, affecting the biodiversity of all species in the food chain and is responsible for physiological changes in some species. Concentration of mere 3 µg/L have negative impacts in the ecosystem biodiversity, the current threshold for ATZ concentration on surface water set by the European Union Directive from 2013 is 2 µg/L.

Nevertheless, society is also directly affected by ATZ contamination. Several health problems are and can be associated with ATZ exposure through drinking water or food contamination. Especially in demographic areas close to agriculture practices were ATZ is used as herbicide, were people living there are expose to high levels of ATZ (WHO, 1990). Also, ATZ is associated to negative effects on menstrual cycle and in hormone levels, fertility problems, osteoporosis, cardiovascular disease and central nervous system deterioration (Cragin et al. 2011)

The reason why ATZ is so prevalent worldwide, even knowing the potential risk and hazards of this chemical, as to do with the economy. ATZ is a low-cost herbicide and shows higher productivity levels when compared with other herbicides. Several studies shown decreases in yield and increases in production costs if ATZ were not used as herbicide (Ackerman, 2007), (Ribaudo,and Bouzaher, n.d.), (USDA - United States Department of Agriculture). Besides, ATZ is very stable when in water and away from sunlight and was found all over central Europe streams in 1979 at levels ranging 0.4 mg/L to 10 mg/L and in surface and groundwater in many states of USA in 1988 (WHO, 1991). Other studies found ATZ in levels close to 6 µg/L in countries around the world (WHO, 1996)

Additionally, a study shows the monitorization of ATZ in a shallow aquifer in western Germany over 20 years. And even after such a long period of time several ATZ metabolites and ATZ were found (see figure 2). This data show by Vonberg et al. (2014) characterizes the stability of ATZ in aquatic environments with low sunlight incidence. Showing the importance for ATZ monitorization even in areas were tis herbicide is no longer used.

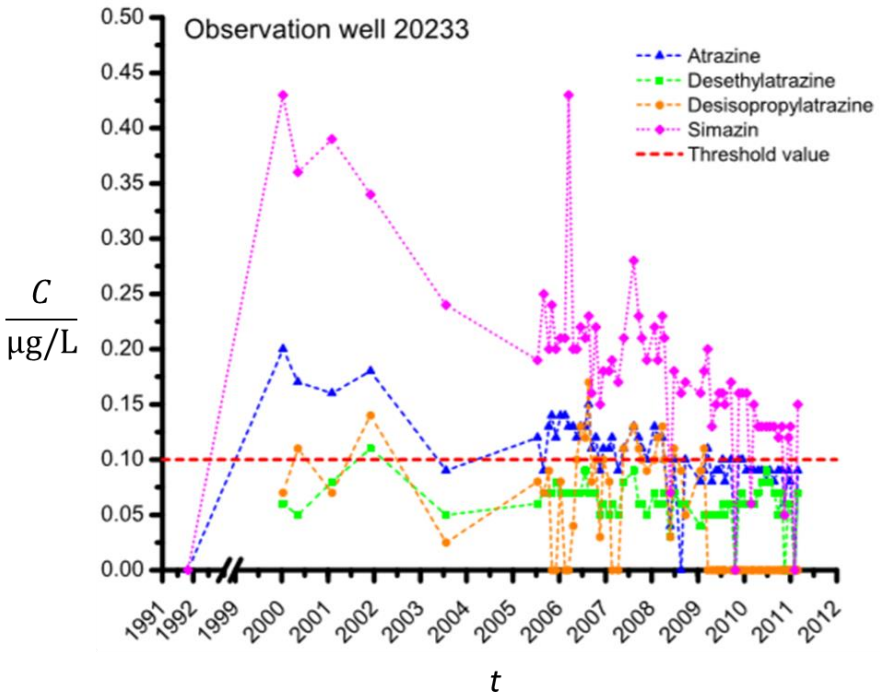

Figure 2. Triazines monitoring from a well in western Germany over 20 years (Vonberg et al., 2014).

1.3 Detection Methods

Recently, many analytical methods were developed, such as gas chromatography–mass spectrometry (Bruzzoniti et al., 2006), ultrasonic solvent extraction coupled with thin-layer chromatography (Rezić et al., 2005) and cloud-point extraction with high-performance liquid chromatography (Urio and Masini, 2016) to detect and quantify ATZ in contaminated samples with very low quantification limits. However, such methods are expensive and time consuming in comparison with sensors base on Molecular Imprinted Polymers (MIPs). MIP-based electrochemical sensors provide a reliable, fast, easy to make and low-cost method to detect ATZ. In table 1, some methods for ATZ quantification are shown. Most of the presented strategies are MIP based and show very low detection limits for ATZ.

Chemical sensors based in MIPs show a promise method for ATZ detection and quantification, as well for other chemicals, several studies show reliable results in this field. MIP-based cartridge for ATZ recognition (Kueseng et al., 2009) and electrochemical sensitive sensor MIP-based for ATZ (Pardieu et al., 2009), are some examples of successful developed MIP's for ATZ recognition. MIPs are a feasible and an economic method in comparison to traditional approaches.

Table 1. Comparison of different methods for ATZ quantification (Yola and Atar, 2017)

Method	**Detection limit**/(μg/L)
MIP/QCM	0.006
MIT/CA	1.725
GC/MIP/SPME	19.843
mixed-bed SPE/ MIP	1.337
MIP/o-PD	0.216
MIP/Au	0.216
MWCNTs/HPLC	0.021
PZC–BSA	0.026
$\mathbf{SiO_2}$/atrazine/MIP	388.224
potentiometric/ MIP	4313.6
biomimetic/MIP	107.840
RAFT-MIPs	2.804
MIP/Pt NPs/ $\mathbf{C_3N_4}$NTs	0.00003

MIP: Molecularly imprinted polymer. QCM: Quartz crystal microbalance. CA: Carbon aerogel. MIT: Molecularly imprinted TiO2. SPME: Solid phase microextraction. GC: Gas chromatography. SPE: Solid microextraction. o-PD: o-Phenylenediamine. Au: Gold. MWCNTs: Multiwalled carbon nanotubes. HPLC: High-performance liquid chromatography. PZC: Piezoelectric quartz crystals. BSA: Bovine serum albumin. SiO2: Silicon dioxide. RAFT: Reversible addition–fragmentation transfer. BiFE: Bismuth film electrode. DPASV: Differential pulse adsorptive stripping voltammetry.

2. GOALS AND FRAMEWORK

This research work was done within the scope of SEALAB project, which aims to develop an automatic system for monitoring priority substances such as pesticides, herbicides and polycyclic aromatic hydrocarbons regulated in EU Directive 2013/39/EU. The automatic system has been integrated into an unmanned vessel and is being tested in a real environment.

ATZ is one of the priority substances listed in EU Directive 2013/39/EU and has been used worldwide in agriculture corps as an herbicide due to is low-cost and effectiveness when compared with other options. However, it has been proved over the years the importance to reduce the use of this

herbicide because the negative impact to the environment and the public health. The traditional methods for ATZ detection and quantification are expensive and time consuming, hence the need for novel strategies that reduce the cost and time procedure. Currently, detection method based on MIPs, provide unique features (easy to use, fast response and inexpensive) that can make it an excellent analytical tool and potentially able for real-time measurements.

2.1 Specific goals

The main goal is to develop an electrochemical MIP based sensing system for detection and quantification of ATZ. And the specific goals defined for this work included a) development of MIPs for biorecognition of ATZ; b) integration of the developed MIPs into an electrochemical sensing system; c) optimization, characterization and evaluation of the developed sensing devices for the detection of ATZ in environmental waters.

2.2 INL (International Iberian Nanotechnology Laboratory) and Water Quality Research Group

The INL, located in Braga (North of Portugal) was founded by the governments of Portugal and Spain under an international legal framework to perform interdisciplinary research, deploy and articulate nanotechnology for the benefit of society. INL aims to become the world-wide hub for nanotechnology addressing society's grand challenges. The research and technology activities are focused on six clusters: Health, Food, Energy, Environment, ICT and Future Emerging Technologies, which complement each other and provide a base for interdisciplinary interactions between researches.

The Water Quality group is one of the twenty-four research groups of INL and is focus on overcoming challenging issues in water environment making responsible use of the opportunities that nanotechnology offers. Such as developing nanotech-based sensors for water quality monitoring, nanomaterials for water contaminants capture and (Eco)nanotoxicology. One of the current ongoing projects is SEALAB that was the motivation for the work performed for this thesis.

3. Bibliographic Revision

In this section MIPs are briefly introduced with some bibliography revision of the subject in question. The general approach for MIP synthesis is explained as well as the theory behind the MIP being developed in this work is for ATZ recognition. Also, some principles and methods of electrochemistry are explained. In general, this chapter tries to clarify some principles and theory essential for the goals define for this work.

3.1 Mass Transport

Before getting into electrochemistry, first it's important to understand the processes that transport molecules or ions in an electrochemical cell. Mass transport can occur by diffusion, when a chemical specie travels through a medium due to the existence of concentration gradients. Diffusion is the spontaneous movement of a particle from high concentration areas to low concentration areas, in order to minimize the concentration differences. Another mass transport phenomenon takes place, when charged species move as consequence of an electric field. Electrostatic forces repeal or attract positive or negative particles. This phenomenon is called migration. It happens in electrolyte cells, when an ion migrates along the electric field generated by the electrodes. At last, convection is the movement of bulk from a high-pressure area to a low-pressure area (Wang, 2000). These three phenomena are illustrated in figure 3.

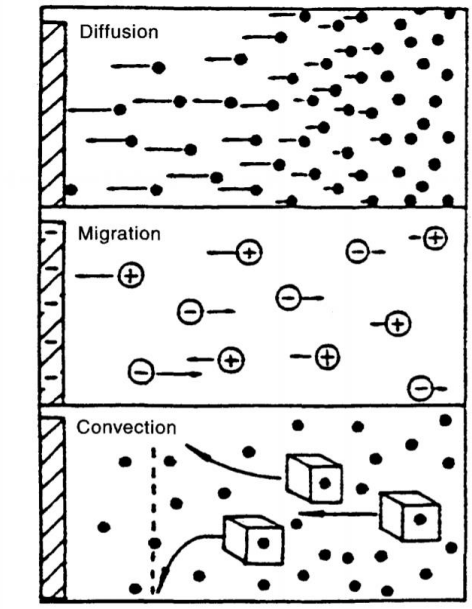

Figure 3. Representation of the mass transport mechanisms (Wang, 2000).

3.2 Electrochemical Cell Mechanism

Electrochemistry studies the relation between chemical reactions and electricity. Redox reactions involve transference of electrons within molecules or ions, one of the reactants is reduce (it gains electrons) at the cathode, the electrode where reduction takes place in an electrochemical cell. And the second reactant is oxidized (it loses electrons) at the anode, the electrode where oxidation takes place in the cell. In electrochemistry, electrons enter the electric circuit through the anode and leave the circuit from the cathode. It's often used to refer as the current generated only by electron-transfer reaction as faradaic current and the current from an electric source as non-faradaic.

Combining this redox reactions in a close electric circuit and a flux of electron can be obtained with an electrolytic cell, if the redox reaction is not spontaneous ($\Delta G > 0$) and a potential differential needs to be applied to the cell, or with a galvanic cell if the redox reactions happen spontaneously ($\Delta G < 0$) generating electric current by itself. The difference and the mechanism of a galvanic cell and an electrolyte cell are explained with more detail in the next sections.

In figure 4, a scheme represents the mechanism of electron transference in an electrolytic cell. Due to electric forces, an oxidized specie is reduced in the cathodic reaction $\mathrm{O} + \mathrm{e}^- \rightarrow \mathrm{R}$, an electron is transferred from the cathode to the reduced specie, R, leaving the electrode. On the other side of the cell, the anodic reaction oxidizes a reduced specie in the oxidation reaction $\mathrm{R} \rightarrow \mathrm{O} + \mathrm{e}^-$, where electrons are transferred to the anode, entering the electric circuit. These two processes, electrons leaving the electric circuit at the cathode and electrons entering the electric circuit at the anode, close the electric circuit allowing a flux of electrons to exist, hence electric current. It's crucial to refer, that these reactions happen on the surface of the electrodes and the electric current is limited by the electron transference related to the kinetics of the redox reaction.

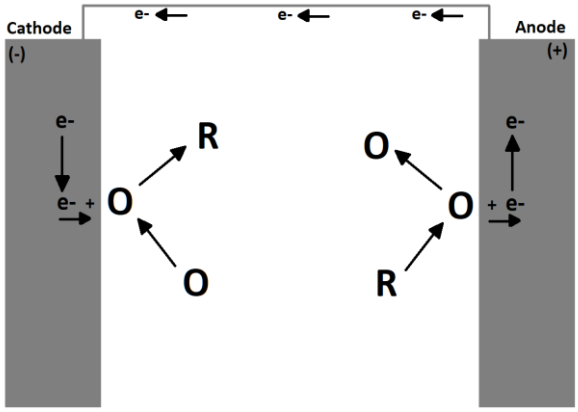

Figure 4. Schematic electrolyte cell mechanism, where O represents the oxidized specie, R characterizes the reduced specie and e- schematizes the electrons.

3.2.1 Electrical Double Layer

To better understand the mechanism of electron transference from a solvated specie in the electrolyte and the electrode surface, is important to imagine an electrical double layer formed at the surface of the electrode. Composed by solvent molecules, solvated ions and partial solvated ions near the surface of the electrode (see figure 5). This double layer is formed when a potential is applied to the electrode and causes a faradaic current to pass through the cell (Zoski, 2007). At this point in time, solvent molecules as well as specifically adsorbed ions (partial solvated) with opposite charge to the electrode are present at the electrode surface, forming the first layer, from the electrode surface to the boundary of the inner Helmholtz plane located at centre of the adsorbed ions (χ_1 in figure 5). The second layer consist of solvated ions that cannot get closer than χ_2 to the electrode surface, is called the outer Helmholtz plane. Which reflects the imaginary plane that passes through the centre of the solvated ions in their nearest point to the electrode surface. These solvated ions are non-specifically adsorbed and are attracted to the surface by electrostatic forces (long range Columbic forces). From outer Helmholtz plane into the bulk, rests the diffusion layer and the ionic species in this plane are less compacted than in the Helmholtz plane (Wang, 2000).

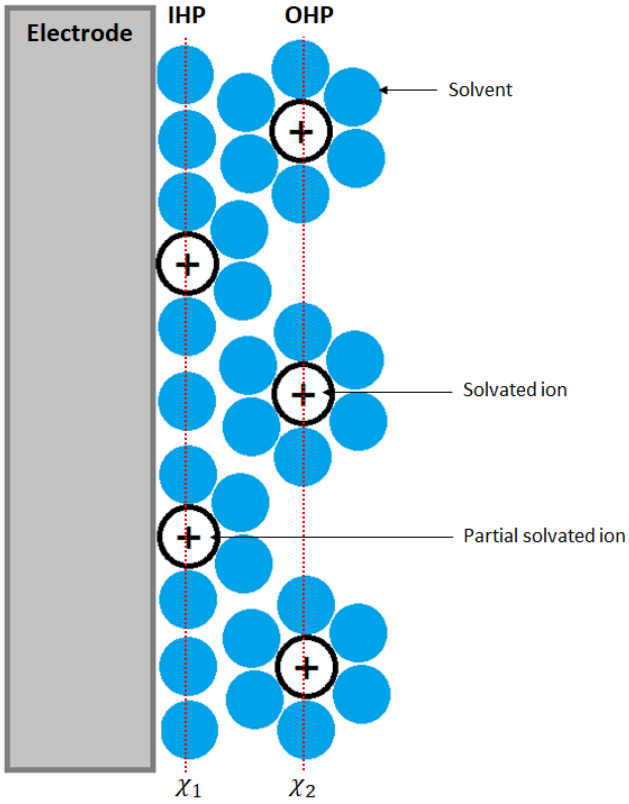

Figure 5. Electric double layer. OHP - outer Helmholtz plane IHP – inner Helmholtz plane.

3.2.2 Electrochemical Cell Design and Electrolytes

Configurations with three electrodes are the most used setup in electrochemistry, it consists in a WE, a RE and a counter electrode (CE). In these cases, the potential is still measured between the WE and the RE, however the current passes through the WE and the CE. Once that just a minimal amount of current, or none, flows through the RE, it becomes more reliable to hold a constant potential over the electrochemical processes.

Nevertheless, all electrochemical phenomena occur in a medium containing dissolved ions which are mobile and able of support current flow. Three properties must be taking into account when choosing a support solution: a) the medium containing mobile ions must contact the electrodes in the electrochemical cell, to allow the control and measurement of the potential in the cell; b) a good solvating power is required in order to dissolve all reactants and products involved in the electrochemical process. To increase mass transport phenomena, low viscosity is also necessary to allow rapid transport of reactants and product to and from the electrode surface. Hence, increasing the kinetics and the productivity of the electrochemical process; c) respectively to the desired reaction, the medium should present low reactivity to avoid secondary processes during the electrochemical reaction of interest (Zoski, 2007).

3.3 Analytical Electrochemistry

Electrochemistry is a powerful branch from analytical chemistry for research and provides technologies to study analytes in solutions, besides being a promise and great option over traditional methods for detection and quantification of low chemicals quantities. It's easily coupled with other novel technologies and provides fast and accurate results and is cheaper than traditional technologies. Techniques like potentiometry and voltammetry are very useful for the studies of redox processes at macro, micro or molecular level using sophisticated instruments (Reedijk and O'Mullane, 2003).

This section briefly introduces some of the voltammetry techniques used in analytical electrochemistry to study redox processes that were used to characterize the MIPs in this work. In short, voltammetry manipulates the potential along a defined range and the current is measured and analysed to obtain information about the analyte. In contrast, potentiometry vary the current and the potential differential in the electrodes is measured with respect to the reference electrode and the working electrode. This last technic was not used in this research project, only voltammetry technics were used and are explained with more detail in the next paragraphs.

3.3.1 Cyclic Voltammetry

Cyclic voltammetry (CV) is the most used technique to obtain qualitative information about an electrochemical reaction (Wang, 2000), in this technic the potential is manipulated linearly over time inside a potential range back and forth and the current is measured versus applied potential. Each new scan has an inverse slope of the previous one, thus a cycle can be obtained. In the example below, figure 6a), the potential off the first scan increases linearly, in time, from -0.1 up to 0.5 V and once it reaches the maximum potential in range it decreases to -0.1 V with the inverse slope of the previous scan. Though, the qualitative information about the electrochemical reaction is obtained when analysing the response of the current versus the potential. Looking at figure 6b), in the forward scan, as the potential approach an value that make the electron-transfer reaction thermodynamically favourable, the current gradually increases, due to the presence of faradic current, till a maximum characteristic of the condition of the systems, in this case at potential 0.15 V (termed oxidation potential). And start to decrease when the applied potential gets more distant from that oxidation potential, because the reducing of faradic current, remaining mostly non-faradaic current. The peak seen at 0.15 V indicates the oxidation potential characteristic of the electrolyte and electrode used. Likewise, for the backward scan as the potential gets closer to a value thermodynamically favourable for the electron-transference between the reductive specie and the electrode, the faradic current increases and start to decrease when the potential gets further from the reduction potential. The resulting plot of current vs potential is termed a cyclic voltammogram and is a complicated, time-dependent function of a large number of physical and chemical parameters (Wang, 2000).

Different electrochemical systems will have different current responses, in the given example the response characterizes the reversible redox process of a system using potassium ferrocyanide and gold electrodes. There are other systems, such as quasi-reversible and irreversible systems. In figure 7, the difference between those systems can be compared. For the irreversible case, only the oxidation peak appears, meaning that the chemical specie is not being reduced in the backward scan of the cyclic voltammetry. In the quasi-reversible case, both oxidation and reduction peaks are found, but are wider and smaller than in the reversible case, meaning that the thermodynamic of the redox reaction is not as favourable as in the reversible case.

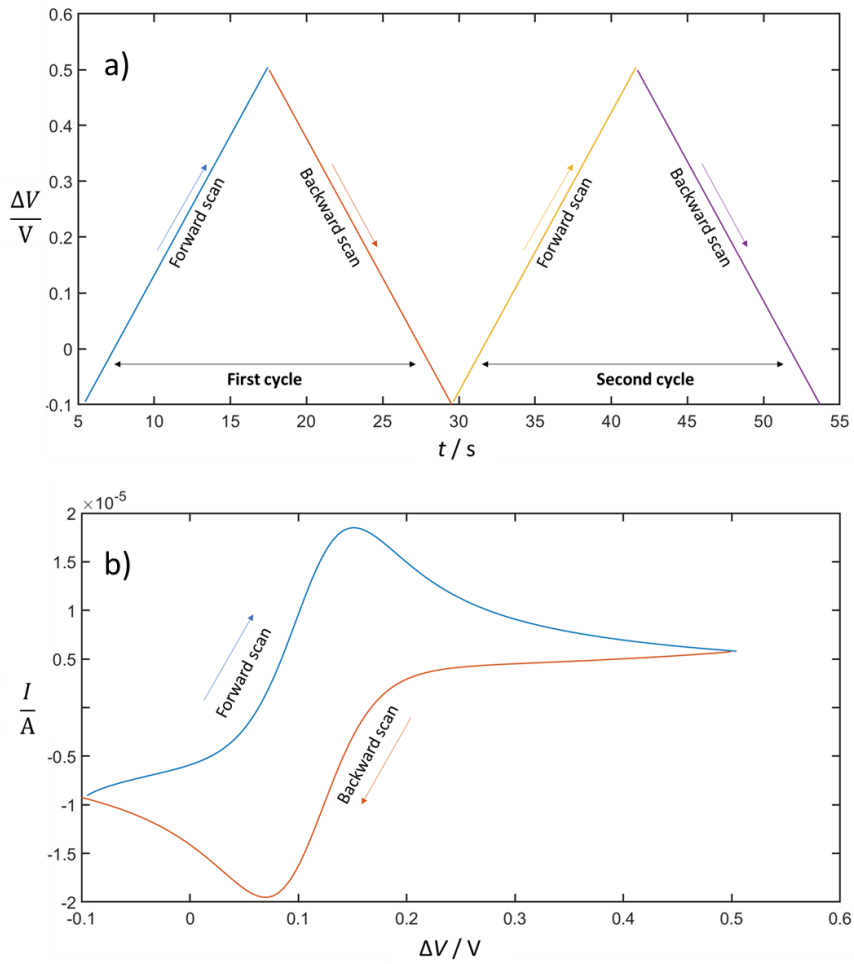

Figure 6. Cyclic voltammetry example. a) potential, ΔV, vs time, t, b) Current, I, vs potential, ΔV.

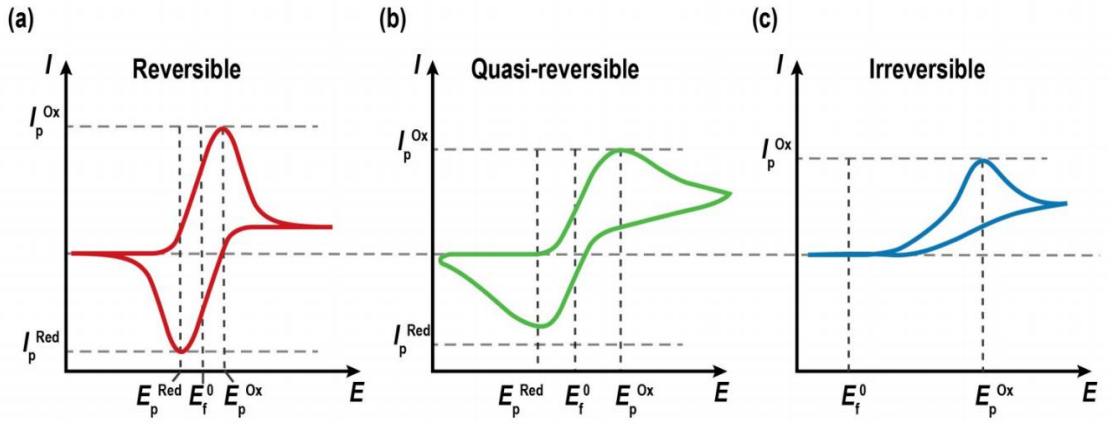

Figure 7. Cyclic voltammograms of reversible, quasi-reversible and irreversible electrochemical systems (Wijeratne, 2019).

3.3.2 Differential Pulse Voltammetry

Pulse voltammetry techniques are focus in lowering the detection limit of electrochemical measurements, differential pulse voltammetry (DPV) is more sensitive than CV and allows detection limits at concentrations as low as 1 µg/L. In DPV, fixed amplitude pulses superimposed on a rising potential ramp are applied to the working electrode. The current is measured twice, before applying the pulse (I_1) and after the pulse (I_2). The first current is instrumentally subtracted from the second, and the difference in currents ($\Delta I = I_2 - I_1$) is plotted versus the applied potential (Wang, 2000). Figure 8A, illustrates the variations of applied potential over time, as well as the ranges of the conditions that are more often used in DPV measurements, while figure 8B plots the ΔI as function of the potential. The closer the potential is to thermodynamically favourable conditions for electron transference processes, the higher the difference between faradaic and non-faradaic currents. When the pulse is applied both currents increase, but due to the redox reaction of the chemical specie the increase in faradaic current is higher than in the non-faradaic, henceforth ΔI increases until a maximum near P_1, after this point the faradaic process begins to be less favourable and the difference $I_2 - I_1$ decreases with the potential.

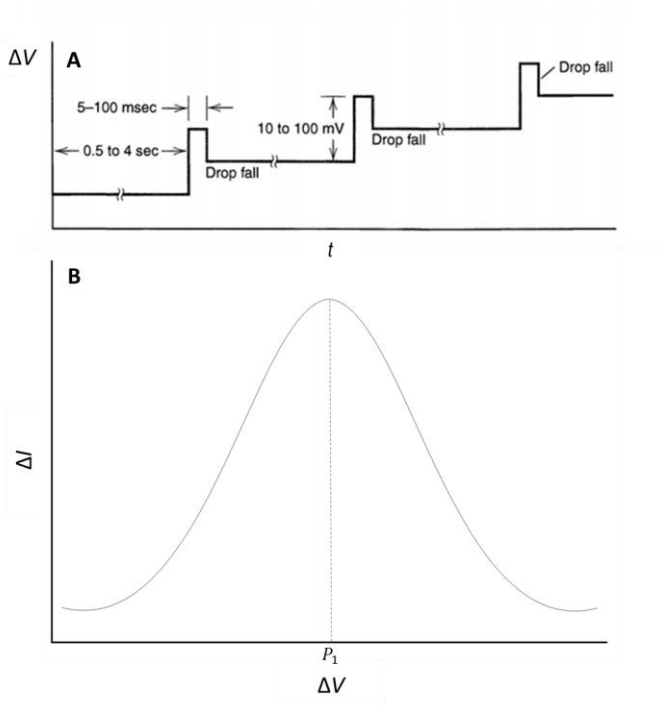

Figure 8. Differential pulse voltammetry applications. A – potential, ΔV, vs time, t (Bard and Faulkner, 2000); B – Current, I, vs potential, ΔV.

3.4 Molecularly Imprinted Polymers

A goal of modern sensor research is the creation of synthetic receptors that mimic the natural antibody–antigen behaviour with similar specificity and sensitivity. This molecular recognition, in combination with modern techniques to monitor changes in the recognition elements, offers the promise of selective, sensitive sensors capable of detecting and monitoring targets. MIPs are best described as synthetic analogues to the natural, biological antibody–antigen systems (BelBruno, 2018), they are tailor-made synthetic materials with artificially generated recognition sites able to specifically rebind a target compound in preference to other closely related compounds. The monomers are chosen based on their capability to interact with the functional groups of the template molecule. Once polymerization is complete, the template molecule is extracted, leaving binding sites with shape, size, and functionalities within the polymer network complementary to the target compound (see figure 9). The resulting imprinted polymers are stable, robust, and resistant to a wide range of pH, solvents, and temperature (Turiel and Esteban, 2020).

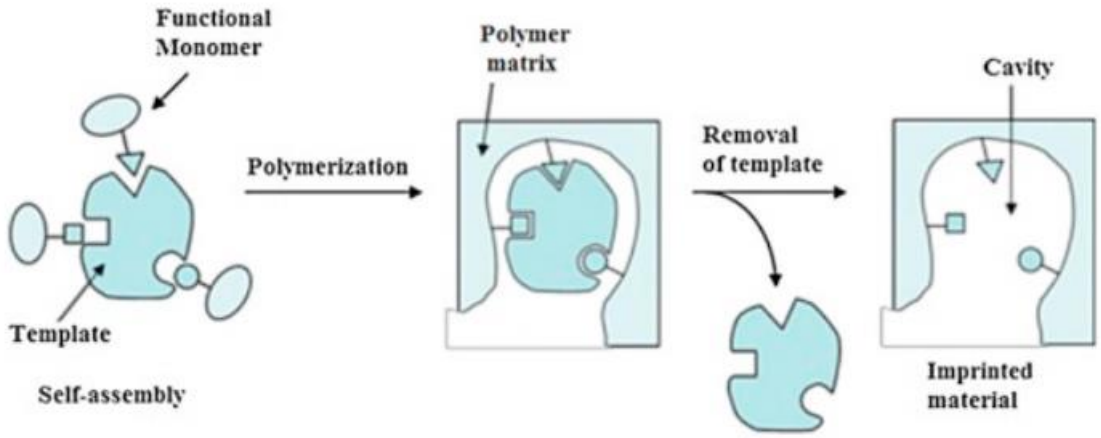

Figure 9. General process for preparation of MIPs (Sellergren, 1999).

3.4.1 MIP Synthesis

There are three general approaches for the synthesis of MIPs: covalent, noncovalent and semi-covalent. In the covalent approach, reversible covalent bonds are formed between complementary functional groups of the monomer and the template before polymerization. Then, these bonds are cleaved to remove the template and are reformed upon rebinding of the target molecule. Similarly, for the semi-covalent approach, the template and the monomer are connected through covalent bounds, but the

rebinding of the template is based in non-covalent interactions. Finally, for the noncovalent approach, both assembly and rebinding are based in weaker bonds between the functional groups of the template and the monomer (Turiel and Esteban, 2020), such as hydrogen bonds. This approach is by far the most common for the preparation of MIPs owing to its simplicity and the availability of a wide variety of monomers (BelBruno, 2018).

The first step in the preparation of MIPs consists in promote the formation of a template-monomer complex in a solvent prior to the polymerization. For that functional group complementary needs to be ensured when choosing the functional monomer, shape complementary is a contributing factor for MIPs recognition (Sellergren, 1999). Hence, for template molecules containing amino groups, such ATZ, monomers containing functional groups capable of forming hydrogen bonds are a good option to promote the template-monomer complex formation. In this work, the functional monomer o-phenylenediamine (o-PD) was chosen, the hydrogen bonds between the amino groups of both template and monomer form a reliable complex, figure 10. Larger numbers of complementary interactions will increase the binding strength and fidelity in the recognition. Thus, templates offering multiple sites of interaction for the functional monomer are likely to yield binding sites of higher specificity and affinity for the template (Sellergren, 1999).

Once the MIP is formed, the template needs to be removed from the polymer matrix to form an imprinted cavity, with specificity in shape, size and interactivity towards the template molecule. Template removal is carried out using solvents capable of disrupt the binding interaction in the template-polymer complex.

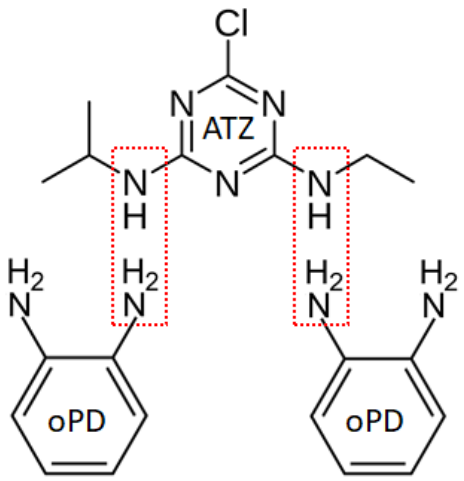

Figure 10. Template-monomer complex hydrogen-bounding interactions. Possible interaction between o-PD and ATZ.

3.4.2 MIP for Atrazine detection

The polymer obtained by electropolymerization of o-PD, has received a great deal of attention, often designated as poly-phenylenediamine. It has several fields of applications such as photovoltaic cells, anticorrosion coatings, pH measurements, electrochemical diodes, corrosion inhibitors, enzyme biosensors and more recently MIPs films (Losito et al., 2003). Is found to adhere to metal surfaces (Brânzoi et al., 2014), resulting in a thin layer of non-conductive polymer with great thermal and chemical stability. Furthermore, the amino groups present in the molecular configuration of this monomer can stablish hydrogen bounds with the amino groups present in ATZ (see figure 10), o-PD was choose as a functional monomer suitable of forming template-monomer interactions before polymerization. Up to five o-PD molecules can interact with one ATZ molecule (Li et al., 2015), hydrogen-bonding can be established with any nitrogen atom in the template molecule. The pre-complex can be electro synthetized, by initiating a chain reaction from an electro radical using an electrochemical cell. The o-PD monomers that are dispersed in the electrochemical solution can be reduced to polymeric forms (Aguilar, 2019). Then CV and DPV, can be employed to analyse the formed polymers.

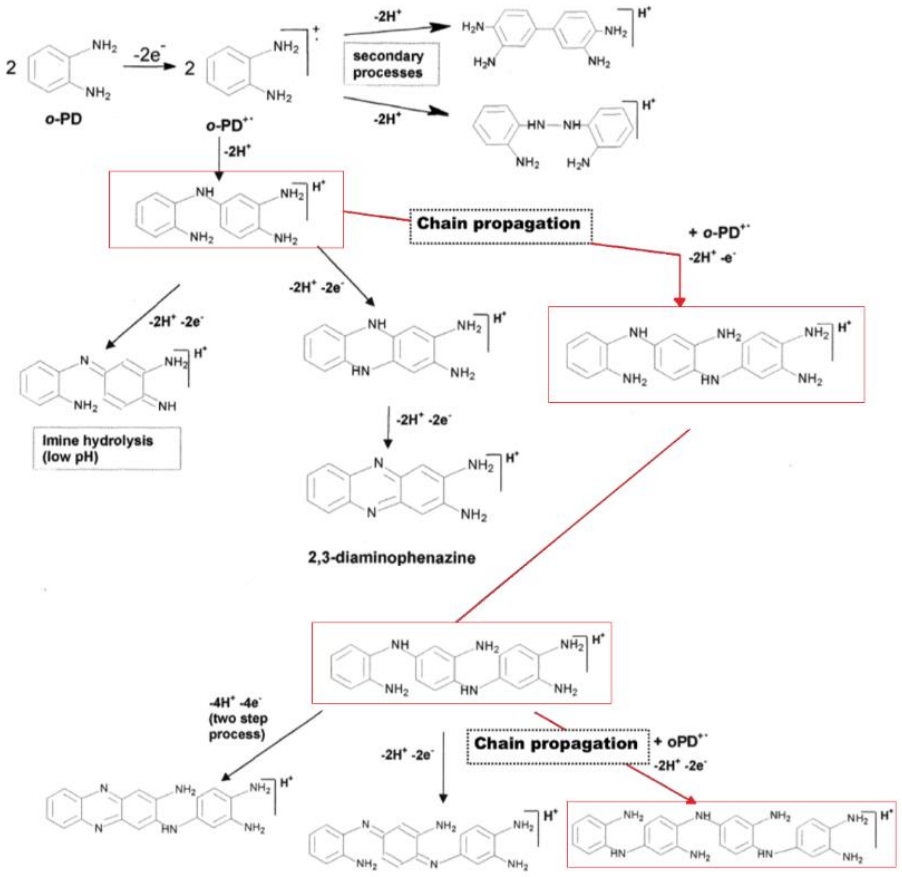

Figure 11. Schematic representation of the o-PD polymerization mechanism. Adapted from Losito et al. (2003).

In detail, the electropolymerization mechanism of o-PD starts from the monomer oxidation followed by radical coupling forming three possible dimers (see figure 11) that can be further oxidised to trimers and so on to higher oligomers promoting the chain propagation. The pH and the potential applied affect the pathways that are followed during electropolymerization. When low values of pH are adopted more dimers are formed, because of the abundance of protonated molecules that will difficult the oxidation process. Hence, higher potentials are needed to ensure the proper oxidation of the molecules to higher oligomers. On the other hand, for higher pH, less protonated molecules are present what boosts oxidation, hence higher oligomers predominate (Losito et al., 2003). Nevertheless, besides pH and potential, the supporting solution upon electropolymerization is also subject of importance and can have major effect on the final polymer (Kiss et al., 2019).

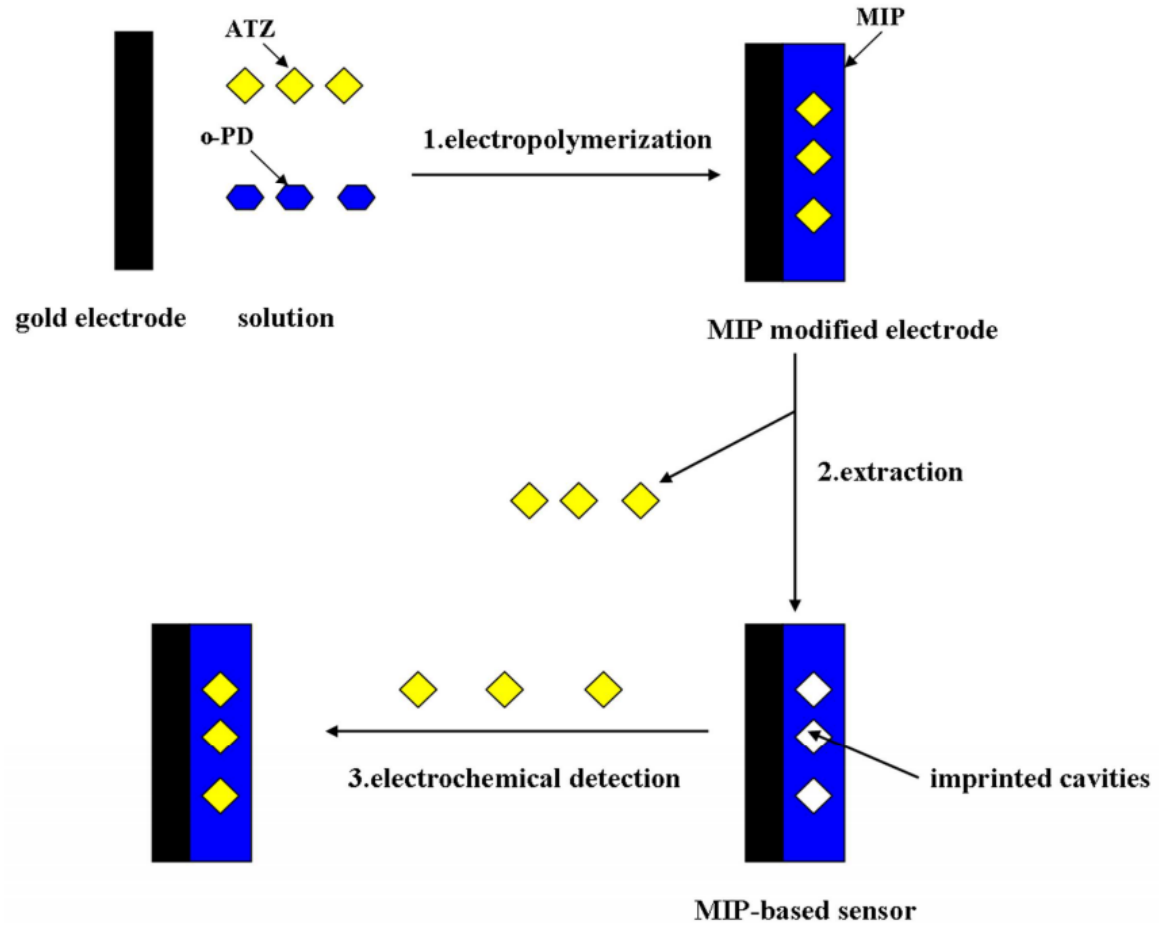

Figure 12. Schematic representation of the steps for MIP synthesis for ATZ detection (Li et al., 2015). Step 1 – electropolymerization; Step 2 – extraction (ATZ removal); Step 3 – electrochemical detection.

Once polymerization complete (see step 1 in figure 12), a thin layer of MIP is attached to the working electrode. ATZ can then be removed from the MIP using solvents capable of disrupt the hydrogen

bond between the complex template-polymer. Protic solvents, such as methanol and water readily donate protons via hydrogen bounds, what makes them good solvents to disrupt the hydrogen-bonding interactions between the template and the polymer (Turiel and Esteban, 2020). After the removal process, imprinted cavities with recognition towards ATZ size, shape and complementarity are left in the polymer matrix (step 2 in figure 12), that can be coupled to electrochemical technics such as CV and DPV to detect very low concentrations of the target molecule in contaminated water samples (step 3 in figure 12).

4. Materials and Methods

4.1 Reagents

Phosphate buffer (PB) pH 7.4, was obtained by preparing two solutions, one with Na_2HPO_4 (obtained from Sigma, Spain), $c(Na_2HPO_4)$ = 0.2 mol/L, and the second with $Na_2H_2PO_4$ (obtained from Sigma, Spain), $c(Na_2H_2PO_4)$. Then using a pH meter, PB pH 7.4 was obtained by adding volumes of the two solutions until a stable value of pH 7.4 was achieved. All water-based solutions were prepared using deionized water (DI) water. Methanol 99.8% (MeOH) obtained from Acros (Spain) and acetic acid (AcOH) from Sigma Aldrich (Spain) were used without further purification, and were used to prepare the extraction solution, containing 9 parts of MeOH and 1 part of AcOH, referred as MeOH:AcOH (9:1, v/v).

For MIP preparation ATZ and o-PD (both obtained from Sigma, Spain) were used without further purification. The solution used for the rebinding of ATZ was prepared by dissolving different amounts of ATZ in DI water containing 1% MeOH.

4.2 Electrochemical-Cell-Chips

The integrated electrochemical detection system used (see figure 13) was composed by microfabricated gold electrodes, like previously detailed in Santos et al. (2019); poly(methyl methacrylate) (PMMA) chambers, a Polydimethylsiloxane (PDMS) O-ring and spring-loaded connectors assembled into a PCB board to stablish the electrical connection to the read-out platform (portable potentiostat).

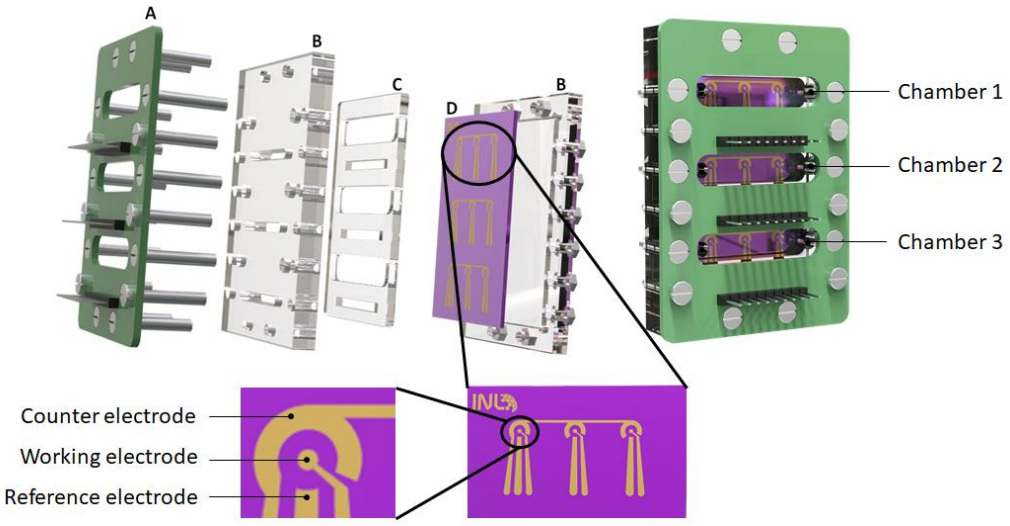

Figure 13. Electrochemical integrated detection system. A) electrical connector; B) PMMA chamber top and bottom parts; C) PDMS O-ring; and D) microfabricated Au sensor.

The Au microfabricated sensor was mounted inside the PMMA chamber, with a PDMS O-ring on top, to protect the electrical connectors, to define the measurement chambers and to prevent fluids leakages.

The integrated electrochemical detection system has three independent chambers of about 300 µL each. Each chamber has an inlet and an outlet for the injection and removal of the solutions necessary during the MIP synthesis, removal of template, rebinding and electrochemical measurements. Each chamber has three electrochemical cells in a three-electrode (CE, WE and RE) configuration, where the CE is common to the 3 cells (inset of figure 13).

4.3 Electrochemical measurements

Electrochemical measurements were performed using a potentiostat (Metrohm Autolab PGSTAT302N) first using screen-printed gold electrodes (SPGE) to optimise MIP synthesis and secondly using the microfabricated sensors. A portable potentiostat, customized for the SEALAB project was also used for the measurements with the microfabricated sensors. All the measurements were carried out using freshly prepared electrolyte solution, containing $K_3[Fe(CN)_6]/K_4[Fe(CN)_6]$ (Sigma, Spain), $c(K_3[Fe(CN)_6]/K_4[Fe(CN)_6])$, and KCl, $c(KCl)$ = 0.1 M, at room temperature.

4.4 MIP preparation

A pre-polymerization solution was prepared by mixing ATZ and o-PD in a PB solution containing 30% of MeOH to dissolve ATZ (c(ATZ) = 1 mmol/L and c(o-PD) = 5 mmol/L), during five hours at 55 rpm. Then, the pre-polymerization solution was injected into the chamber and the system was submitted to 15 cycles of CV scans, between 0 and 0.8 V, at a scan rate of 0.05 V/s and a step of 0.01 V, in order to electropolymerized the dissolved complex (see step 1 in figure 12) on the surface of the gold electrode. Then, freshly made solution of MeOH:AcOH (9:1, v/v) was used to disrupt the hydrogen bounds and extract ATZ from the polymer matrix (see step 2 in figure 12), during 15 min. Parallel to the MIP preparation, a non-imprinted polymer (NIP) was also prepared in similar conditions but without ATZ, to form a polymer without cavities for the recognition for ATZ, that is used as control.

4.5 Analytical performance of MIP-based electrochemical sensors

Solutions containing ATZ, like detailed in 4.1, were injected (300 µL) inside the electrochemical chamber for 8 min to rebind the ATZ molecules in the polymer matrix. Then CV and DPV were performed to study the rebinding of ATZ in the MIP. DPV was performed in potential range between -0.5 and 0.5 V, with a step of 0.005 V, a modulation amplitude of 0.025 V, a modulation time of 0.05 s and 0.2 s as interval time. CV measurements were performed between -0.5 V and 0.5 V, with 0.005 V as step at a 0.05V/s scan rate. Both, CV and DPV were carried out in freshly made electrolyte solution, previously described.

4.6 Characterization Methods

4.6.1 Ultra-High-Performance Liquid Chromatography (UHPLC)

UHPLC measurements were performed in Agilent 1290 Infinity II LC HPLC system (Waldbronn, Germany). The UHPLC was equipped with a pump module, a vacuum degasser, an autosampler, a thermostatted column compartment, and a diode-array detector (DAD). Data acquisition was performed by Agilent's ChemStation software, version 1.9.0. Reverse phase analysis was carried out with a Kinetex EVO C-18 column purchased from Phenomenex (Madrid, Spain) (reversed phase, particle size of 2.6 µm, pore size of 100 Å, length 100 mm, internal diameter 4.6 mm). The mobile phase used was MeOH:AcOH (9:1, v/v) at a flow rate of 1 mL/L and an injection volume of 20 µL. The detection was carried out at 230 nm in a UV detector after 2 min of elution.

4.6.2 Atomic Force Microscopy (AFM)

AFM Dimension Icon (Bruker, USA) was used in tapping mode and measurements were performed in air using a tip with nominal frequency of 240 kHz. The linear scanning rate was set between 0.5 and 1 Hz, with scan resolution of 512 samples per line. Surface roughness analysis was performed on the topography images. It is expressed as the root mean square roughness and the roughness average (*Ra*, arithmetic average of the absolute values of the roughness profile ordinates) of height deviations taken from mean image data plane. Analyses were carried out using commercial AFM software from Bruker.

4.6.3 Scanning electron microscopy

Scanning electron microscopy (SEM) analysis of the electrode surface was carried out on a FEI Quanta 650 FEG (FEI Europe B.V.) using an electron acceleration voltage of 20 kV (high vacuum mode), at 60 Pa and spot size of 3. Secondary electrons were detected by an Everhardt Thornley SED (secondary electron detector).

5. Results Discussion

5.1 MIP preparation optimization

Electrochemical measurements were performed using CV scans between -0.5 and 0.5 V, with scan rate of 50 mV/s in a solution, *c*(KCL) = 0.1 mol/L and *c*($K_3[Fe(CN)_6]/K_4[Fe(CN)_6]$) = 5 mmol/L.

5.1.1 Electropolymerization conditions optimization

Several electropolymerization conditions were studied and optimized, using SPGEs, to achieve the best performance of the ATZ MIP-based sensor. One of the main problems early found during this work, was the low ATZ solubility in water (0.15 mM). To overcome this, two approaches were tested: a) add an organic solvent, such as MeOH in the pre-polymerization solution to increase the solubility of ATZ; and b) reduce the concentration of ATZ in the electropolymerization step to a value soluble in water. For that, different pre-polymerization solutions were prepared: i) one prepared in PB (pH 7.34) designated as PPS1 (pre-polymerization solution one); ii) a second prepared in PB containing 42.5% MeOH (PPS2 in figure 14), where the both contained *c*(ATZ) = 1 mmol/L and *c*(o-PD) = 5 mmol/L; and iii) a third solution prepared in PB (pH 7.34) with *c*(ATZ) = 0.15 mmol/L and *c*(o-PD) = 0.75 mmol/L (PPS3 in figure 14). The objective was to ensure the complete dissolution of ATZ in the solvent used while maintaining the same ratio between ATZ and o-PD (1:5), in order to get the most stable complex between template and monomer.

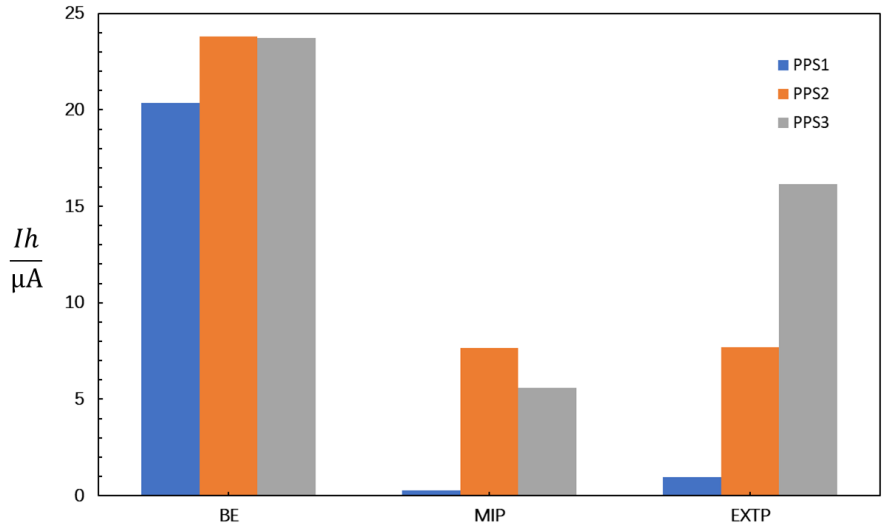

Figure 14. Peak height, *Ih*, variation over the different steps in MIP synthesis, using different pre-polymerization solutions (PPS1, PPS2 and PPS3). BE: bare electrode; MIP: molecularly imprinted polymer; EXTP: extracted polymer.

Three pre-polymerization solutions were studied using CV and according to figure 14, the MIP with PPS1 shows smaller peak heights values than the MIP prepared from PPS2 and PPS3. Taking into account that the concentration of o-PD in PPS3 was lower than in PPS1, the amount of available monomer may not have been enough for the electropolymerization, hence a thinner layer of MIP is formed allowing a higher flow of current when comparing with the MIP synthetized with PPS1, resulting in a higher peak height value.

Comparing the PPS1 with PPS2, it can be seen from figure 14 that PPS2 has a higher peak value than PPS1. The presence of MeOH to dissolve ATZ in PPS2 could influence the final polymer structure, resulting in the difference between PPS1 and PPS2. In this case, the amount of o-PD was the same in PPS1 and PPS2, however the MeOH in PPS2 increase the porosity of the polymer matrix, resulting in a MIP with a higher porosity that will facilitate the current flow. This can explain the signal difference for the MIPS prepared from PPS1 and PPS2.

Next, the extraction of ATZ was also studied. In all the cases the extraction was in a PB solution for 15 min. For PPS1 and PPS2, the results show that the EXTP (see EXTP in figure 14) does not show any significant difference after the extraction step, what was suggested by the similarity in the signals of the EXTP and the MIP, for each case. For example, in PPS1 the difference between MIP and EXTP is 0.71 μA, which is very low. The same happens for PPS2, where the difference is almost none (0.04 μA).

In the extraction step, ATZ molecules should be removed from the matrix leaving empty imprinted cavities, which facilitate the flow of electrons through the electrode surface. This is reflected in an increase of the signal at the EXTP. However, this did not happen in the case of PPS1 and PPS2, where a higher difference was expected when compared with the MIP signal. This is an indicator that ATZ was not removed completely from the binding sites. The small variation shown by the results can be associated with: i) the amount of ATZ that is being retained in the polymer during the electropolymerization, is much lower than the expected, resulting in a small amount of ATZ imprinted in the MIP, hence when the analyte is removed from the polymer few cavities are formed; or that ii) the extraction solution is not sufficient enough to remove ATZ from the cavity sites.

For the PPS3, the results show that ATZ is being removed from the MIP, what is in accordance with the very high variation between the signal of the EXTP and the MIP ($\Delta i_p \approx 10$ μA). The extraction had a bigger impact in the PPS3 case, because of the less compact polymer film that may be a result of the lower o-PD concentration. In this case, ATZ could be more expose to the extraction solution, facilitating its removal.

The results obtained, show that PPS2 is the best pre-polymerization solution, because it maximizes the number of imprinted cavities in the MIP, produces a more robust layer than PPS3 and is able to dissolve a higher amount of ATZ.

In the next section, the best conditions for ATZ extraction were optimized.

5.1.2 Extraction conditions optimization

According to the previous results, the extraction step requires further optimization. For that, two polymers were prepared using PPS2. Then, two different solutions were used to extract ATZ, i) a PB solution (EXT-PB) and ii) a PB solution with 30% MeOH (EXT-MeOH). The former was used to increase the solvation power of the extraction solution (see figure 15). Both, were used for 15 min.

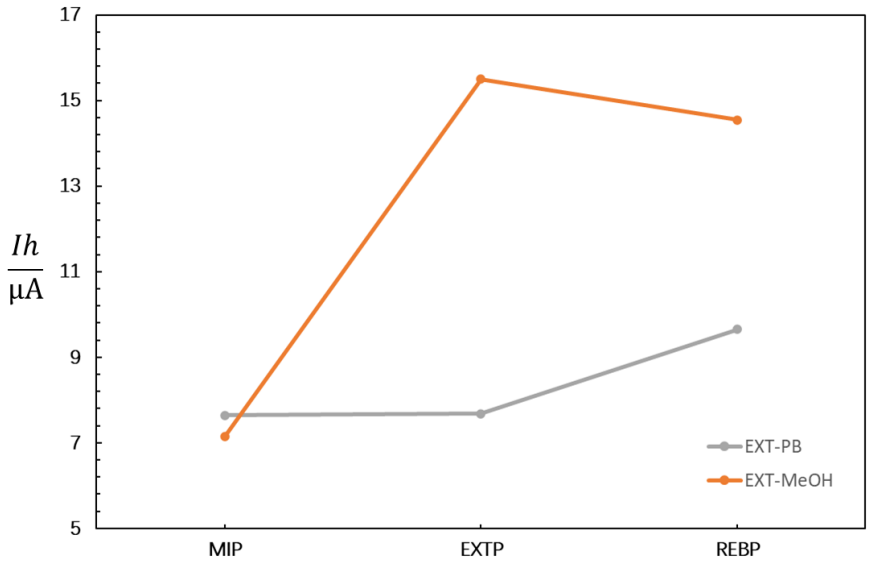

Figure 15. Peak height, *Ih*, variation for extraction optimization in SPGE. Comparison between two different extraction solutions (EXT-MeOH and EXT-PB). Measurement conditions: CV between -0.5 and 0.5 V at scan rate of 50 mV/s. MIP: polymer; EXTP: extracted polymer; REBP: rebounded polymer.

According to figure 15, the results show a clear difference between the two cases. The EXT-MeOH had a higher impact in the EXTP signal than the EXT-PB, suggesting that ATZ is being removed. This may happen because the higher solvation power of the EXT-MeOH, acquired from the presence of MeOH. The solubility of ATZ in MeOH is much higher than in PB, hence the EXT-MeOH solution enables the removal ATZ more efficiently than the EXT-PB solution.

Next, the rebinding of ATZ was performed. The results show a decreasing trend for EXT-MeOH and an increasing trend for EXT-PB. The decreasing trend suggest that ATZ is rebinding to the MIP. Hence, MeOH increases the extraction efficiency and shown to be crucial to achieve a good MIP performance.

Besides EXT-MeOH and EXT-PB, other extraction solutions were studied, such as NaOH (*c*(NaOH) = 0.25 mol/L) and AcOH. However, the hydroxide reacted with the electrode passivation layer, Al_2O_3, and AcOH seemed to completely remove the polymer from the electrode surface. Hence, these two extraction solutions were rejected.

5.1.3 Electrode properties influence in MIP performance

For the optimization of the MIP synthesis, SPGEs were used. In this section, two different electrodes were studied and compared, SPGEs and Au microfabricated sensors. In this section, the properties of different electrodes that could influence the MIP performance were studied (see figure 16).

The main differences of SPGEs and the microfabricated electrodes are the materials composition of the electrodes, size, and surface roughness. The SPGEs are composed with a WE and a CE, made of a gold paint, while in the Au microfabricated sensor the electrodes are metal gold, deposited by physical vapour techniques (Santos et al., 2019). Also, the RE in SPGEs is made of a silver paint, while in the Au microfabricated sensor is made of gold. Moreover, the surface of the three electrodes, WE, CE and RE, have different sizes, the SPGE displays a WE with a diameter of 1.6 mm and the WE of the Au microfabricated sensor displays a diameter of 0.95 mm (Santos et al, 2019). Finally, the surface roughness of both electrodes is very different, the SPGEs present a *Ra* of 0.5 µm (information provided in Dropsens material's datasheet) while the Au microfabricated sensor surface is much smoother, with a *Ra* lower than 5 nm. According to Butterworth et al. (2019), the roughness is one of the characteristics that affects the sensor performance.

In the SPGE the high surface roughness, could be influencing the stability of the layer, in figure 16 it can be seen a less homogenous surface for the SPGE, with a lot of defects, that could negatively influence the attachment of the MIP layer to the gold surface. On the other hand, in the microfabricated sensors the smother surface supports the adhesion of the MIP layer.

Since the MIP layer onto the microfabricated sensors is more robust, another extraction solution was tested, MeOH:AcOH (9:1, v/v) from Li et al. (2015). The comparison between the *Ih* performed in the SPGE and in the ECC are displayed in table 2.

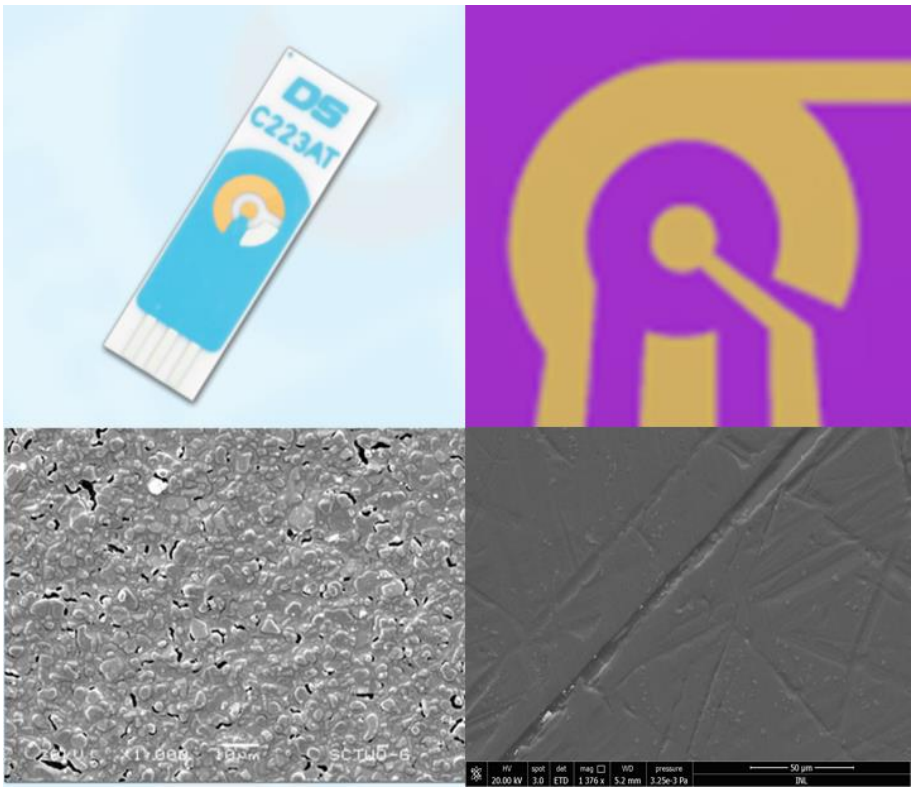

Figure 16. Differences between SPGEs (left) and Au microfabricated sensors (right). SEM images of the surface of both sensors.

The results in table 2, show the stability of the MIP onto the microfabricated electrode. The extraction solution seems to be removing the layer from the SPGE surface, however, in the microfabricated sensors, the ATZ extraction is suggested by the increase of the signal after the extraction. Hence, MeOH:AcOH (9:1, v/v), was chosen as the best extraction solution for the removal of ATZ from the polymer matrix using the microfabricated sensors. From the conducted studies, it was noted that the MIP layer was more stable when electropolymerized onto the ECC surface.

Table 2. Comparison of the extraction peak height signal, *Ih*, in SPGE and microfabricated sensors. All data in µA. Measurement conditions: CV between -0.5 V and 0.5 V at scan rate of 50 mV/s. BE: bare electrode; MIP: polymer; EXTP: extracted polymer

	SPGE	ECC
BE	20.9	8.8
MIP	0.4	0.05
EXTP	20.3	5.4

5.1.4 UHPLC results

UHPLC was performed to identify the presence of ATZ in the extraction solution. The results are displayed in figure 17. And show a peak at 2.091 min that relates to ATZ, meaning that ATZ is being detected in the extraction solutions. Thus, confirming the extraction of ATZ from the MIP, using MeOH:AcOH (9:1, v/v) as extraction solvent.

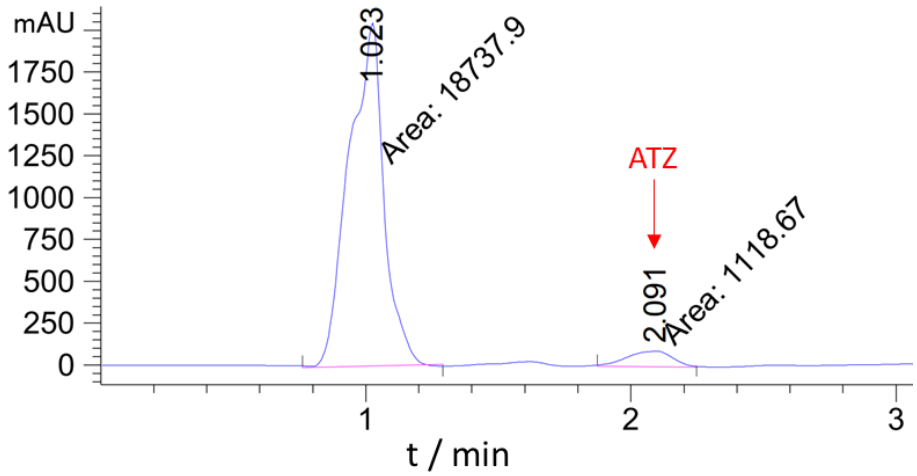

Figure 17. ATZ retention peak in UHPLC.

5.2 MIP and NIP characterization

In this section, MIP and NIP were characterized using electrochemical techniques and advanced characterization techniques such as SEM and AFM for the characterization of the surface of the polymers.

5.2.1 Electrochemical characterization

MIP and NIP were electropolymerized over fifteen consecutive CV scans into the microfabricated sensors, as shown in figure 18. In both, two peaks are seen, that corresponded to the oxidation potential of o-PD (Öndeş and Soysal, 2019), meaning that polymer structures are being formed (see figure 11). The decreasing trend of these peaks heights over the CV scans suggest that the electrode surface is being covered by the growing polymer chain. And according to the very low current range of the last cycles, it can be concluded that a non-conductive polymer layer was formed onto the WE of the sensor.

A difference is seen between the polymerization for MIP and NIP synthesis, that can be associated with the presence of ATZ in the pre-polymerization solution for MIP.

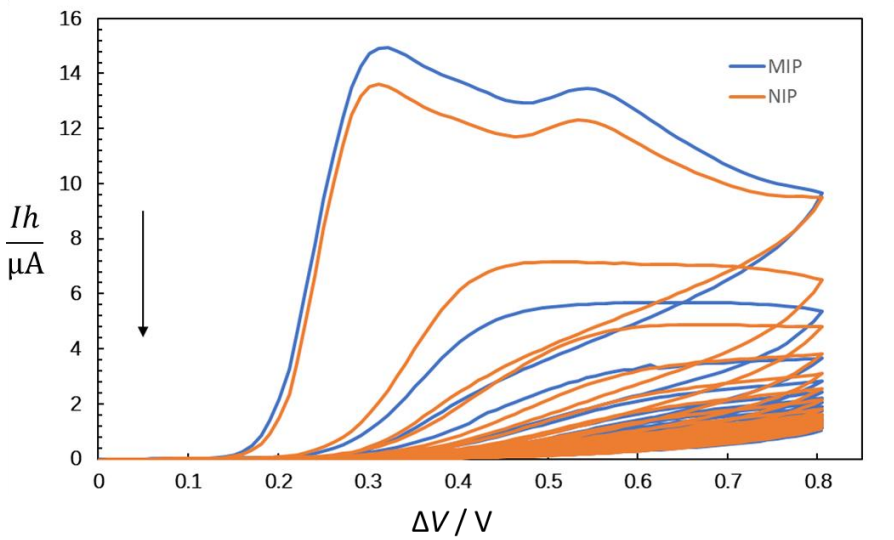

Figure 18. Electropolymerization of MIP and NIP. Current, I, vs potential, ΔV. Electropolymerization conditions: *c*(ATZ) = 1 mmol/L, *c*(o-PD) = 5 mmol/L in PB:30 % MeOH over 15 cycles between 0 and 0.8 V at 50 mV/s scan rate.

In figure 19, are shown the CV scans for the different steps of the polymer preparation. Both cases show the typical redox peaks of ferricyanide probe (*c*($K_3[Fe(CN)_6]/K_4[Fe(CN)_6]$) = 5 mmol/L) that decreases to near zero after electropolymerization of o-PD in the electrode surface (MIP/NIP in figure 19), what suggests the formation of a non-conductible film onto the electrode surface and is in line with the polymerization results in figure18. However, both MIP and NIP show similar signals for each of the steps, other studies have demonstrated bigger differences between MIP and NIP (Öndeş and Soysal, 2019), (Li et al., 2015), (Shoji et al., 2003). However, after the rebinding of 33 mg/L of ATZ (REBP in figure 19) both MIP and NIP current signal decreases. In the MIP the rebinding of ATZ into the imprinted cavities is expected to block the current flow, resulting in the decrease of the current signal. Since the NIP does not have imprinted cavities ATZ may be bonding to the surface of the polymer and thus inducing the reduction of the current signal of the NIP.

5.3 MIP-based electrochemical sensor analytical performance

5.3.1 DPV characterization

DPV responses for different concentrations of ATZ for rebinding in MIP are displayed in figure 20. The DPV curves show a clear decreasing trend with the increase in ATZ concentration. These results are consistent with theory, since for higher concentration of ATZ more cavities are filled, difficulting the flow of current. Resulting in lower current responses for higher concentrations.

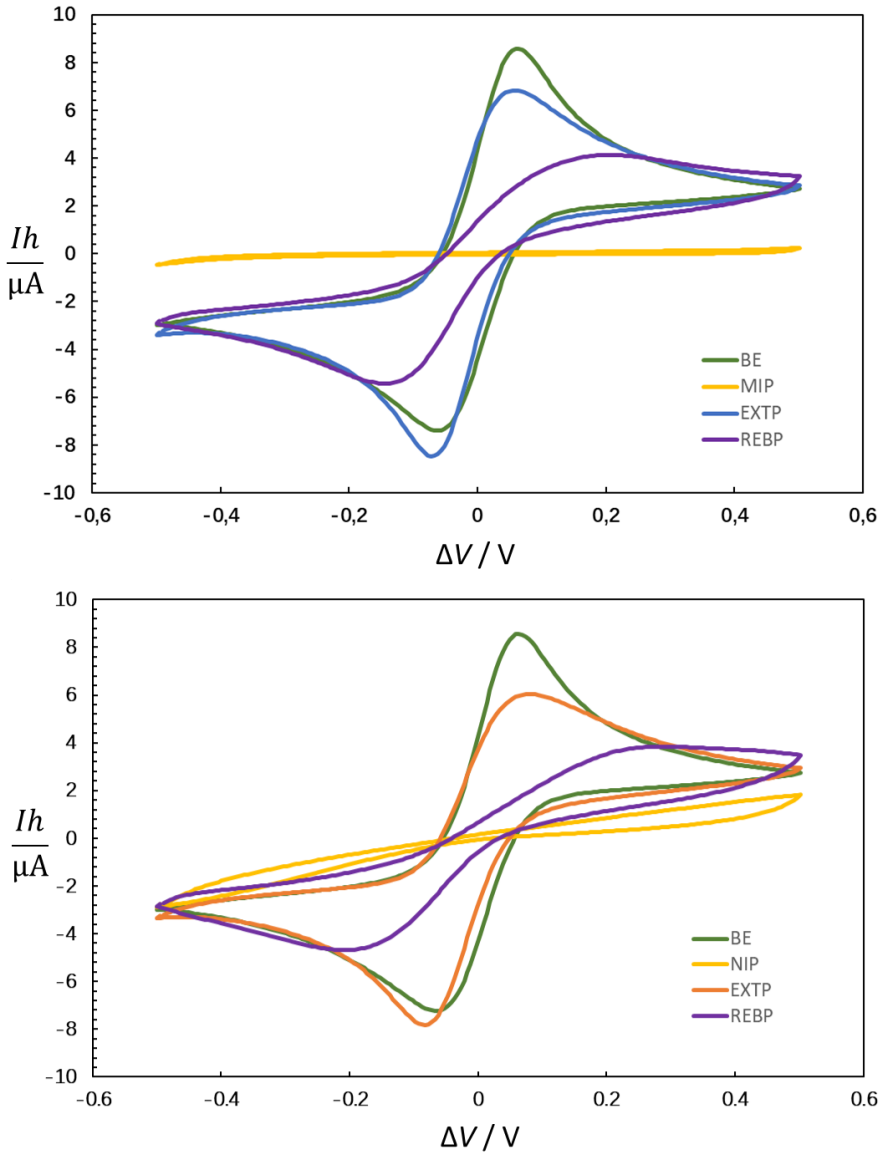

Figure 19. CV characterization of MIP (A) and NIP (B).Current, *I*, vs potential, *ΔV*. CV scan between -0.5 V and 0.5 V at 50 mV/s scan rate in ferricyanide, *c* = 5 mmol/L. BE: bare electrode; MIP: molecularly imprinted polymer; NIP: non-molecularly imprinted polymer EXTP: polymer after extraction; REBP: polymer after rebinding of ATZ.

Several concentrations of ATZ were used in detection. The results show that the signal variation for MIP between 10 µg/L, 25 µg/L and 50 µg/L (see green, purple curves and black curves in figure 20) is lower than the variation between 0 and 10 µg/L. This could suggest that the saturation of the imprinted cavities is being reached around 10 µg/L.

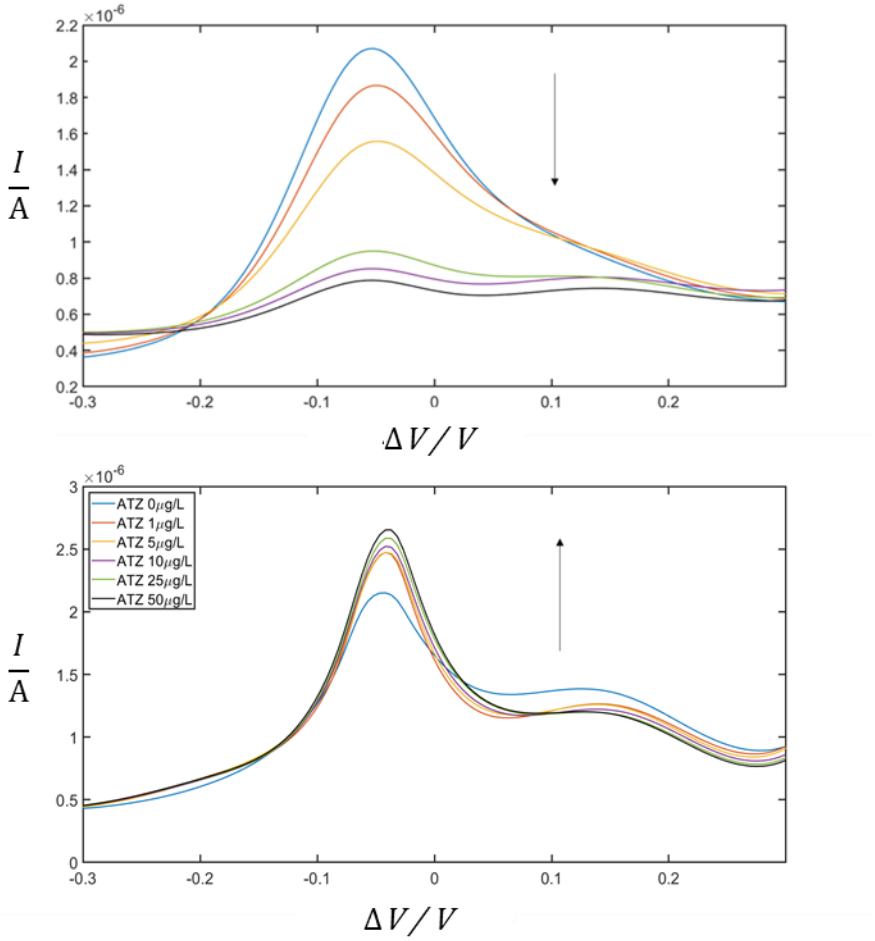

Figure 20. DPV curves of MIP (top) and NIP (bottom) for different concentration of ATZ (i → j): (0, 1, 5, 10, 25, 50 µg/L). Measurement conditions: DPV between -0.5 and 0.5 V. Modulation time: 0.05 s; Interval time: 0.2 s; Amplitude: 0.05 V; Step: 0.05 V.

5.3.2 Calibration curve

The analytical performance of MIP and NIP were evaluated by the measurement of the peak current variation against varying concentrations of ATZ. A calibration curve (see figure 21), current vs concentration, was then calculated for MIP and NIP by the analysis of DPV peaks obtained (see figure 20). It was found a dynamic range between 0 and 25 µg/L with a limit of detection (LOD) of 1.63 µg/L, according to equation 1 (Kumar and Pavan, 2012), for MIP. Sy is the standard deviation of the regression curve and S is the slope of the curve. In this dynamic range, the sensor showed a high sensitivity, towards ATZ recognition.

$$\mathrm{LOD} = 3.3 \times \frac{\mathrm{Sy}}{\mathrm{S}} \qquad (1)$$

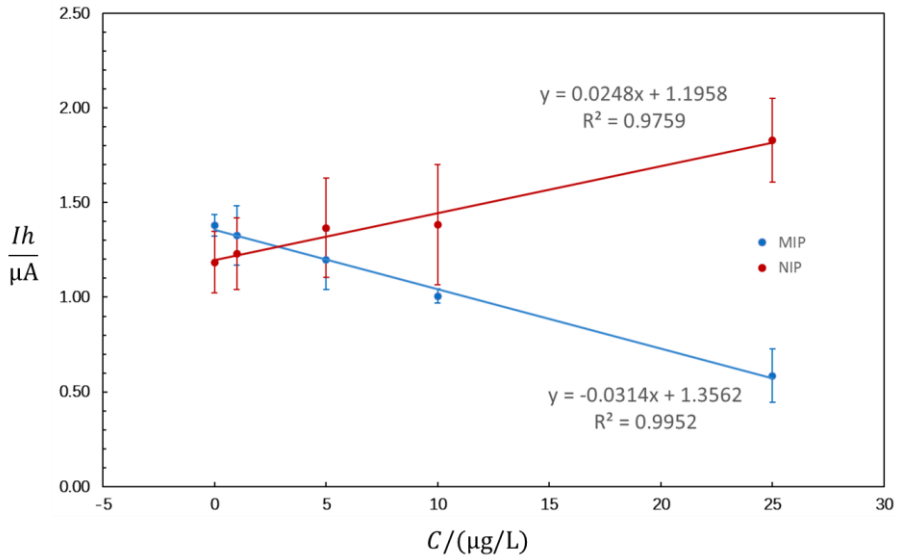

Figure 21. Calibration curve for MIP and NIP in ECC. Peak height, *Ih*, vs concentration, *C*. Measurement conditions: DPV between -0.5 and 0.5 V; Modulation time: 0.05 s; Interval time: 0.2 s; Amplitude: 0.05 V; Step: 0.05 V. n=3.

The results show a clear difference in the MIP and NIP trends. The negative slope in the MIP case is in line with what is expected, higher ATZ concentrations result in lower current signals because the filling of the imprinted cavities. NIP shows a completely opposite trend and less accurate. The MIP trend is a good indicator of ATZ recognition in water samples. Moreover, the difference between NIP and MIP trends suggest that ATZ is binding to the imprinted cavities. Nonetheless, the LOD is lower than the threshold of 2 µg/L define by the EU water directive (EC, 2013), which means that the developed MIP sensor shows promising results for the detection of low ATZ concentration in real water samples.

5.4 Seawater samples

The final sensor application is to detect ATZ in seawater and the current results were performed in DI water. So, seawater samples were tested, and the result were compared with signal obtained in DI water samples. Figure 22 displays the results regarding the detection of ATZ in seawater with a salinity of about 35 mg/L. According to the obtained results, the detection signal is higher in seawater than in DI water, what can be explained by the salinity of seawater. The more ionic species are present, the higher the conductivity of the liquid, resulting in a higher measured signal.

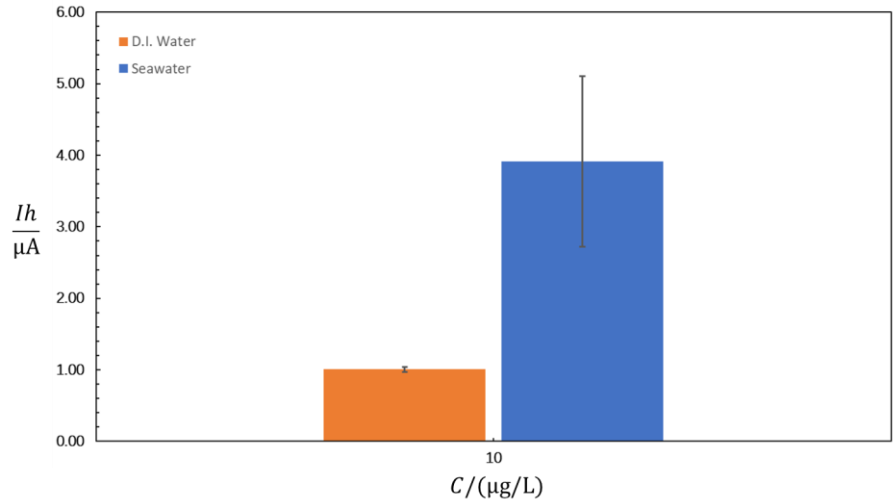

Figure 22. Comparison between ATZ peak height signal, *Ih*, in DI water and seawater. Measurement conditions: DPV between -0.5 and 0.5 V; Modulation time: 0.05 s; Interval time: 0.2 s; Amplitude: 0.05 V; Step: 0.05 V. n=2.

5.5 Polymer Stability

The polymer stability for consecutive extractions and rebinding cycles was studied with CV. The goal was to understand the signal variations between consecutive extractions and rebinding cycles. Hence, four cycles (extraction and rebinding) were performed and the CV results are presented in figure 23.

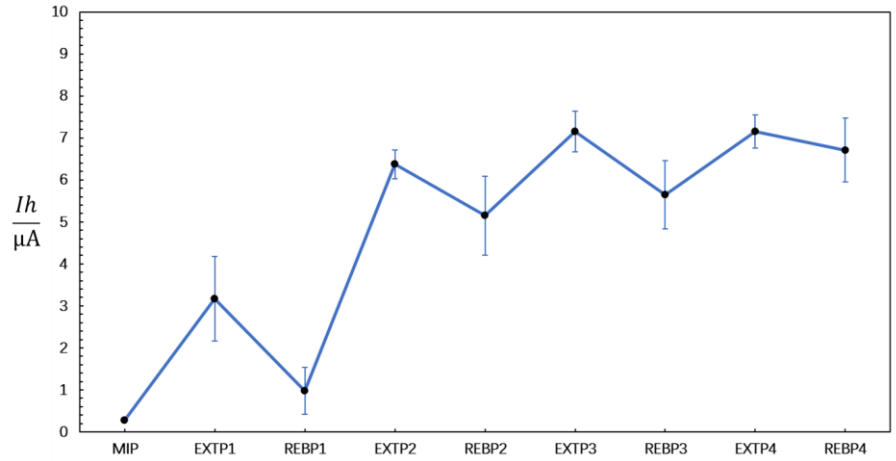

Figure 23. Peak height, *Ih*, variation vs extraction and rebinding cycles for MIP sensor. EXTP: extracted polymer; REBP: rebinding. Measurement conditions: CV scan between -0.5 V and 0.5 V at 50 mV/s scan rate in ferricyanide, *c* = 5 mmol/L. n=3.

Successive extraction and rebinding cycles were performed with a MIP. The results in figure 23, show decreasing in the signal for the REBP1 to a value (0.97 μA) close to the MIP before extraction

(0.28 μA). After the second extraction EXTP2 show an expressive increase in the signal (see table 3). Despite this increase, the REBP2 shows a reduction in the signal, suggesting the rebinding of ATZ. For the second and third cycle, the variations between the EXTP and the REBP are in the same magnitude order.

According to the results displayed in figure 23 the MIP show a slight increasing trend over the consecutive cycles what could indicate the loss of sensibility towards ATZ recognition. Still, this is expected because the wear caused by the consecutive extractions of ATZ from the imprinted cavities, what might reduce the interaction between the functional groups of both the polymer and the template.

In table 3, the signal variation along the extraction and rebinding cycles is displayed. According to the results, it is clear that the signal has a higher variation between the first and second cycle (Δ1 in table 3), what could indicate that the first extraction was inefficient and many ATZ molecules were still present in the polymer matrix. After the second cycle, the variations are less what indicates that the MIP is more stable. Overall, the MIP shows a good stability over the consecutive cycles, meaning that the polymer is reliable to detect ATZ more than one time.

Table 3. Variation between rebinding cycles signals: $\Delta 1 = I_{REBP2} - I_{REBP1}$; $\Delta 2 = I_{REBP3} - I_{REBP2}$; $\Delta 3 = I_{REBP4} - I_{REBP3}$. Data in μA

	Δ1	Δ2	Δ3
REBP	4.17	0.50	1.06
EXTP	3.20	0.78	0.00

5.6 Characterization Methods (SEM and AFM)

AFM analysis was performed to study the variation in the roughness of the electrode surface during the steps for MIP synthesis. According to AFM results, displayed in figure 24, it is evident the variation of the roughness at the electrode surface. The BE shows a *Ra* of (1.73 ± 0.44) nm and after the polymerization the surface exhibits a *Ra* of (2.18 ± 0.73) nm. This increasing in the roughness is an indicator of the formation of a film at the electrode surface. After the extraction of ATZ the roughness slightly increases to a *Ra* value of (2.63 ± 1.44) nm (EXTP in figure24), what suggests the removal of ATZ from the cavity sites. The removal of ATZ from the polymer matrix, leaves imprinted cavities on the layer, what increases the roughness of the surface.

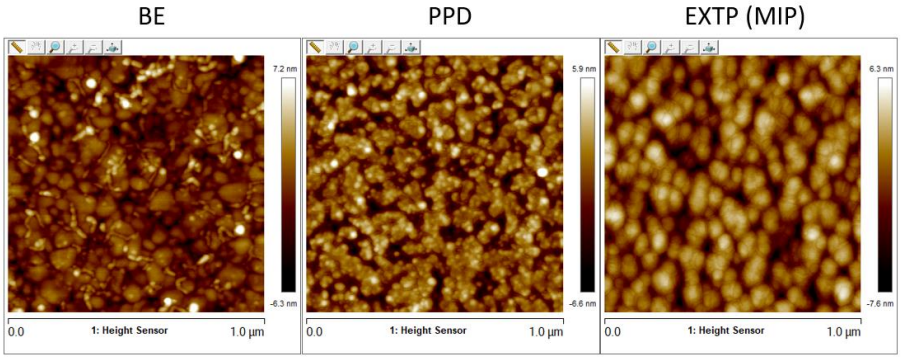

Figure 24. AFM images of the surface of the bare electrode (BE), electrode modified with MIP and after extraction of ATZ (EXTP).

In line with the hypothesis shown by AFM, SEM imaging also shown the formation of a polymer layer at the electrode surface. From figure 25, a clear difference can be seen between the BE and the MIP, a material is covering the gold surface, suggesting that MIP was electropolymerized onto the electrode gold surface.

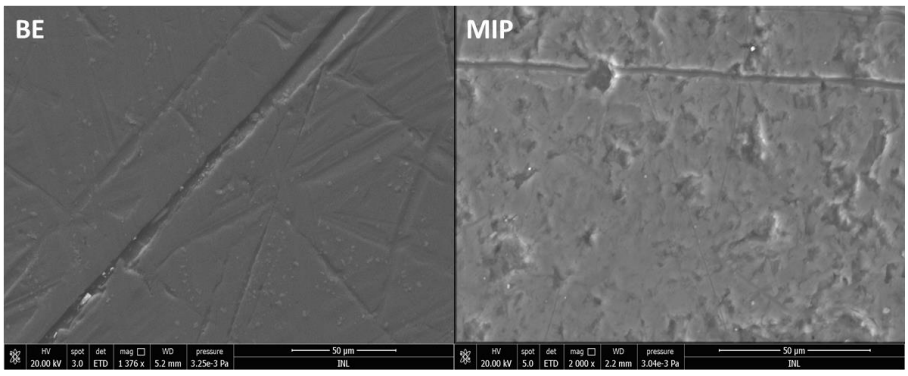

Figure 25. SEM images of the bare electrode (BE) on the left; and MIP modified electrode on the right.

5.7 MATLAB code for peak search in CV and DPV data

A code in MATLAB was developed to analyse the graphical data from the CV and DPV measurements obtained from the portable read-out platform. The code was than translated to PYTHON to be incorporated in a novel device to automatically analyse the data collected from CV and DPV measurements. The program can calculate the peak height, the potential where the peak appears, the peak area and the peak width at half height of CV and DPV scans. The MATLAB version of this program was used to calculate all the data displayed in this report related to electrochemical measurements. Metrohm Autolab PGSTAT302N provides a software (NOVA 2.1) specific for electrochemical data analysis.

However, due to the amount of data measured the MATLAB program show to be faster than NOVA 2.1 and similarly accurate, as it can be seen in table 4. Besides, the MATLAB program can analyse data from different file formats, especially data from the read-out platform, what cannot be done with NOVA 2.1, because the software can only read NOX files. This is a great advantage because the program can be integrated in a real time detection system and providing accurate results.

Table 4. Comparison between results calculated in MATLAB program and NOVA 2.1

	Example 1		**Example 2**	
Parameters	**MATLAB**	**NOVA**	**MATLAB**	**NOVA**
Peak Potential / V	0.177	0.177	0.089	0.089
Peak Height / µA	19.847	20.034	8.681	8.738
Width at Half Height / V	0.171	0.179	0.161	0.154
Area below Peak	3.886	4.018	1.738	1.630

6. Conclusion

In this work a MIP-based electrochemical sensor was developed for ATZ recognition and quantification in seawater. The optimization experiments show that the use of MeOH is necessary to dissolve ATZ, prior to the electropolymerization and that the presence of MeOH is also important for the extraction step. MeOH influences the porosity of the polymer matrix, resulting in the formation of a more porous matrix. Still, MeOH shows to be the best strategy to overcome the low solubility issue of ATZ when compared with the other strategies studied.

The electrodes properties have major impacts on the MIP performance. The MIP assembled in the microfabricated sensor seems to be more stable and homogeneous, allowing the use of stronger solvents. UHPLC measurements show the presence of ATZ in the extraction solution, what indicates that ATZ is being removed from the polymer matrix.

SEM and AFM results show the differences associated with the electrode's modifications performed after the electropolymerization and after the extraction of ATZ. SEM shows a clear difference of the electrode surface, after the electropolymerization, associated to the presence of a MIP layer. AFM results also indicated the formation of a layer on the electrode surface and also suggest ATZ removal from the cavities sites.

The CV characterization results related to electropolymerization are in line with the results seen in the SEM and AFM analysis. Furthermore, CV also shown differences in the polymerization of MIP and NIP, suggesting that ATZ is present during the electropolymerization solution for MIP synthesis.

The analytical performance of the sensor, shows a dynamic range between 0 and 25 µg/L, and a LOD of 1.63 µg/L. A calibration curve was extracted for MIP and NIP, the decreasing trend in MIP case suggests that ATZ is being detected using the developed sensor. NIP results show an opposite trend of the MIP, which is in agreement with the correct function of the sensor. For values of ATZ around 10 µg/L the signal obtained shows a possible saturation of the imprinted cavities. Furthermore, there is a variation between the signal obtained from DI water and seawater. Still, the sensor seems a promising strategy for ATZ detection in seawater.

Moreover, a program was successfully developed in MATALB for electrochemical results analysis. When compared with NOVA 2.1, the program shows similar accuracy, it can use data from different files formats from other devices, is faster to analyse big groups of data and it can be integrated in a real-time system for ATZ detection.

In general, the technique developed in this work proves, that MIP based sensors are a promising strategy to detect and quantify ATZ in real-time. Besides the need for more optimization, this technique shows potential to be a reliable, reusable, low-cost and easy to prepare sensor for ATZ recognition.

7. References

Ackerman, F. (2007). The Economics of Atrazine. *International Journal of Occupational and Environmental Health*, *13*(4), 437–445. https://doi.org/10.1179/oeh.2007.13.4.437

Aguilar, L. E. (2019). Nanotechnology in improving medical devices for smart drug delivery. In C. H. Park, C. S. Kim, A. R. K. Sasikala, & A. R. Unnithan (Eds.), *Biomimetic Nanoengineered Materials for Advanced Drug Delivery* (pp. 73–90). Elsevier Gezondheidszorg.

Amistadi, M. K., Hall, J. K., Bogus, E. R., & Mumma, R. O. (1997). Comparison of gas chromatography and immunoassay methods for the detection of atrazine in water and soil. *Journal of Environmental Science and Health, Part B*, *32*(6), 845–860. https://doi.org/10.1080/03601239709373116

Bard, A. J., & Faulkner, L. R. (2000). Differential pulse voltammetry. In *Electrochemical Methods* (p. 286). Wiley.

BelBruno, J. J. (2018). Molecularly Imprinted Polymers. *Chemical Reviews*, *119*(1), 94–119. https://doi.org/10.1021/acs.chemrev.8b00171

Boundy-Mills, K. L., de Souza, M. L., Mandelbaum, R. T., Wackett, L. P., & Sadowsky, M. J. (1997). The atzB gene of Pseudomonas sp. strain ADP encodes the second enzyme of a novel atrazine degradation pathway. *Applied and Environmental Microbiology*, *63*(3), 916–923. https://doi.org/10.1128/aem.63.3.916-923.1997

Brânzoi, V., Pilan, L., & Brânzoi, F. (2004). Electropolymerization Mechanism and Electrochemical Behaviour of Poly(o-phenylenediamine) film Synthesized in the Presence and Absence of some Surfactants. *Molecular Crystals and Liquid Crystals*, *416*(1), 61–72. https://doi.org/10.1080/15421400490482899

Bruzzoniti, M. C., Sarzanini, C., Costantino, G., & Fungi, M. (2006). Determination of herbicides by solid phase extraction gas chromatography–mass spectrometry in drinking waters. *Analytica Chimica Acta*, *578*(2), 241–249. https://doi.org/10.1016/j.aca.2006.06.066

Butterworth, A., Blues, E., Williamson, P., Cardona, M., Gray, L., & Corrigan, D. K. (2019). SAM Composition and Electrode Roughness Affect Performance of a DNA Biosensor for Antibiotic Resistance. *Biosensors*, *9*(1), 22. https://doi.org/10.3390/bios9010022

Cragin, L. A., Kesner, J. S., Bachand, A. M., Barr, D. B., Meadows, J. W., Krieg, E. F., & Reif, J. S. (2011). Menstrual cycle characteristics and reproductive hormone levels in women exposed to atrazine in drinking water. *Environmental Research*, *111*(8), 1293–1301. https://doi.org/10.1016/j.envres.2011.09.009

Dropsens. (n.d.). Screen-printed gold electrodes. Metrohm DropSens. Retrieved February 5, 2021,from http://www.dropsens.com/en/pdfs_productos/new_brochures/gold_elect rodes.pdf

Esteban, A. M., & Sellergren, B. (2012). Molecularly Imprinted Polymers. In J. Pawliszyn (Ed.), *Comprehensive Sampling and Sample Preparation: Analytical Techniques for Scientists* (pp. 331–344). Elsevier.

EC (2013). European Commision Directive 2013/39/EU

Graymore, M., Stagnitti, F., & Allinson, G. (2001). Impacts of atrazine in aquatic ecosystems. *Environment International*, *26*(7–8), 483–495. https://doi.org/10.1016/s0160-4120(01)00031-9

Holme, T. A. (n.d.). *Denaturation - Chemistry Encyclopedia - structure, proteins, metal, salt*. Chemstry Explained, Foundations and Applications. Retrieved December 31, 2020, from http://www.chemistryexplained.com/Co-Di/Denaturation.html

Kiss, L., Bősz, D., Kovács, F., Li, H., Nagy, G., & Kunsági-Máté, S. (2019). Investigation of phenol electrooxidation in aprotic non-aqueous solvents by using cyclic and normal pulse voltammetry. *Polymer Bulletin*, *76*(11), 5849–5864. https://doi.org/10.1007/s00289-019-02678-2

Kueseng, P., Noir, M. L., Mattiasson, B., Thavarungkul, P., & Kanatharana, P. (2009). Molecularly imprinted polymer for analysis of trace atrazine herbicide in water. *Journal of Environmental Science and Health, Part B*, *44*(8), 772–780. https://doi.org/10.1080/03601230903238319

Kumar, G. S., & Pavan, B. S. K. (2012). Stability-indicating RP-HPLC method for determination of tamsulosin HCL in pharmaceutical dosage form. Journal of Basic and Clinical Pharmacy, 3(2), 255. https://doi.org/10.4103/0976-0105.103817

Lerch, R. N., Donald, W. W., Li, Y.-X., & Alberts, E. E. (1995). Hydroxylated Atrazine Degradation Products in a Small Missouri Stream. *Environmental Science & Technology*, *29*(11), 2759–2768. https://doi.org/10.1021/es00011a010

Li, X., He, Y., Zhao, F., Zhang, W., & Ye, Z. (2015). Molecularly imprinted polymer-based sensors for atrazine detection by electropolymerization of o-phenylenediamine. *RSC Advances*, *5*(70), 56534–56540. https://doi.org/10.1039/c5ra09556e

Losito, I., Palmisano, F., & Zambonin, P. G. (2003). o-Phenylenediamine Electropolymerization by Cyclic Voltammetry Combined with Electrospray Ionization-Ion Trap Mass Spectrometry. *Analytical Chemistry*, *75*(19), 4988–4995. https://doi.org/10.1021/ac0342424

Marchetti, G., Minella, M., Maurino, V., Minero, C., & Vione, D. (2013). Photochemical transformation of atrazine and formation of photointermediates under conditions relevant to sunlit surface waters: Laboratory measures and modelling. *Water Research*, *47*(16), 6211–6222. https://doi.org/10.1016/j.watres.2013.07.038

Minero, C., Pelizzetti, E., Malato, S., & Blanco, J. (1996). Large solar plant photocatalytic water decontamination: Degradation of atrazine. *Solar Energy*, *56*(5), 411–419. https://doi.org/10.1016/0038-092x(96)00028-x

Moreira, A. J., Borges, A. C., Gouvea, L. F. C., MacLeod, T. C. O., & Freschi, G. P. G. (2017). The process of atrazine degradation, its mechanism, and the formation of metabolites using UV and UV/MW photolysis. *Journal of Photochemistry and Photobiology A: Chemistry*, *347*, 160–167. https://doi.org/10.1016/j.jphotochem.2017.07.022

Öndeş, B., & Soysal, M. (2019). Determination of Diuron by Using Electrochemical Sensor Based on Molecularly Imprinted Polymer Film. *Journal of The Electrochemical Society*, *166*(6), B395–B401. https://doi.org/10.1149/2.0631906jes

Pardieu, E., Cheap, H., Vedrine, C., Lazerges, M., Lattach, Y., Garnier, F., Remita, S., & Pernelle, C. (2009). Molecularly imprinted conducting polymer based electrochemical sensor for detection of atrazine. *Analytica Chimica Acta*, *649*(2), 236–245. https://doi.org/10.1016/j.aca.2009.07.029

Reedijk, J., & O'Mullane, A. P. (2013). Electrochemistry. In *Reference Module in Chemistry, Molecular Sciences and Chemical Engineering* (p. n/A). Elsevier Gezondheidszorg.

Rezić, I., Horvat, A. J. M., Babić, S., & Kaštelan-Macan, M. (2005). Determination of pesticides in honey by ultrasonic solvent extraction and thin-layer chromatography. *Ultrasonics Sonochemistry*, *12*(6), 477–481. https://doi.org/10.1016/j.ultsonch.2004.07.004

Ribaudo, M. O., & Bouzaher, A. (n.d.). Atrazine: Environmental Characteristics and Economics of Management. Resources and Technology Division, Economic Research Service, U.S. Department of Agriculture. Agricultural Economic Report No. 699.

Rodriguez, V. M., Thiruchelvam, M., & Cory-Slechta, D. A. (2005). Retracted: Sustained Exposure to the Widely Used Herbicide Atrazine: Altered Function and Loss of Neurons in Brain Monoamine Systems. *Environmental Health Perspectives*, *113*(6), 708–715. https://doi.org/10.1289/ehp.7783

Sagarkar, S., Mukherjee, S., Nousiainen, A., Björklöf, K., Purohit, H. J., Jørgensen, K. S., & Kapley, A. (2013). Monitoring bioremediation of atrazine in soil microcosms using molecular tools. *Environmental Pollution*, *172*, 108–115. https://doi.org/10.1016/j.envpol.2012.07.048

Santos, M. B., Queirós, R. B., Geraldes, Á., Marques, C., Vilas-Boas, V., Dieguez, L., Paz, E., Ferreira, R., Morais, J., Vasconcelos, V., Piteira, J., Freitas, P. P., & Espiña, B. (2019). Portable sensing system based on electrochemical impedance spectroscopy for the simultaneous quantification of free and total microcystin-LR in freshwaters. *Biosensors and Bioelectronics*, *142*, 111550. https://doi.org/10.1016/j.bios.2019.111550

Sellergren, B. (1999). Polymer- and template-related factors influencing the efficiency in molecularly imprinted solid-phase extractions. *TrAC Trends in Analytical Chemistry*, *18*(3), 164–174. https://doi.org/10.1016/s0165-9936(98)00117-4

Shoji, R., Takeuchi, T., & Kubo, I. (2003). Atrazine Sensor Based on Molecularly Imprinted Polymer-Modified Gold Electrode. *Analytical Chemistry*, *75*(18), 4882–4886. https://doi.org/10.1021/ac020795n

Singh, S., Kumar, V., Chauhan, A., Datta, S., Wani, A. B., Singh, N., & Singh, J. (2018). Toxicity, degradation and analysis of the herbicide atrazine. *Environmental Chemistry Letters*, *16*(1), 211–237. https://doi.org/10.1007/s10311-017-0665-8

Szalewicz, K. (2003). Hydrogen bond. In R. A. Meyers (Ed.), *Encyclopedia of Physical Science and Technology* (3rd ed., pp. 505–538). Academic Press.

Turiel, E., & Esteban, A. M. (2020). Molecularly imprinted polymers. In C. F. Poole (Ed.), *Solid-Phase Extraction (Handbooks in Separation Science)* (1st ed., pp. 215–233). Elsevier.

Urio, R. P., & Masini, J. C. (2016). Determination of Simazine and Atrazine in River Water by Cloud-Point Extraction and High-Performance Liquid Chromatography. *Analytical Letters*, *50*(7), 1065–1074. https://doi.org/10.1080/00032719.2016.1212203

Vonberg, D., Vanderborght, J., Cremer, N., Pütz, T., Herbst, M., & Vereecken, H. (2014). 20 years of long-term atrazine monitoring in a shallow aquifer in western Germany. *Water Research*, *50*, 294–306. https://doi.org/10.1016/j.watres.2013.10.032

Vonberg, D., Hofmann, D., Vanderborght, J., Lelickens, A., Köppchen, S., Pütz, T., Burauel, P., & Vereecken, H. (2014). Atrazine Soil Core Residue Analysis from an Agricultural Field 21 Years after Its Ban. *Journal of Environmental Quality*, *43*(4), 1450–1459. https://doi.org/10.2134/jeq2013.12.0497

Wang, J. (2000). *Analytical Electrochemistry*. Wiley.

Wijeratne, K. (2019). *Conducting Polymer Electrodes for Thermogalvanic Cells*. Amsterdam University Press.

WHO. (1991) – World Health Organization – IARC Monographs on the evaluation of carcinogenic risks to humans. *International Agency for Research on Cancer. Occupational exposures in insecticide applications and some pesticides.* IARC Lyon France.

WHO. (1996) – World Health Organization -. Atrazine in Drinking-water Background document for development of WHO Guidelines for Drinking-water Quality. Food and Agriculture Organization. https://www.who.int/water_sanitation_health/dwq/atrazinerev0305.pdf

Yola, M. L., & Atar, N. (2017). Electrochemical Detection of Atrazine by Platinum Nanoparticles/Carbon Nitride Nanotubes with Molecularly Imprinted Polymer. *Industrial & Engineering Chemistry Research*, *56*(27), 7631–7639. https://doi.org/10.1021/acs.iecr.7b01379

Zoski, C. G. (2007). *Handbook of Electrochemistry*. Elsevier Gezondheidszorg.

Annex A

List of priority substances regulated in EU/directive/2013.

AA: annual average.

MAC: maximum allowable concentration.

Unit: [µg/l] for columns (4) to (7)

[µg/kg wet weight] for column (8)

(1)	(2)	(3)	(4)	(5)	(6)	(7)	(8)
No	Name of substance	CAS number (1)	AA-EQS (2) Inland surface waters (3)	AA-EQS (2) Other surface waters	MAC-EQS (4) Inland surface waters (3)	MAC-EQS (4) Other surface waters	EQS Biota (12)
(1)	Alachlor	15972-60-8	0,3	0,3	0,7	0,7	
(2)	Anthracene	120-12-7	0,1	0,1	0,1	0,1	
(3)	Atrazine	1912-24-9	0,6	0,6	2,0	2,0	
(4)	Benzene	71-43-2	10	8	50	50	
(5)	Brominated dipheny-lethers (5)	32534-81-9			0,14	0,014	0,0085
(6)	Cadmium and its compounds (depending on water hardness classes) (6)	7440-43-9	≤ 0,08 (Class 1) 0,08 (Class 2) 0,09 (Class 3) 0,15 (Class 4) 0,25 (Class 5)	0,2	≤ 0,45 (Class 1) 0,45 (Class 2) 0,6 (Class 3) 0,9 (Class 4) 1,5 (Class 5)	≤ 0,45 (Class 1) 0,45 (Class 2) 0,6 (Class 3) 0,9 (Class 4) 1,5 (Class 5)	
(6a)	Carbon-tetrach-loride (7)	56-23-5	12	12	not applicable	not applicable	
(7)	C10-13 Chloro-alkanes (8)	85535-84-8	0,4	0,4	1,4	1,4	
(8)	Chlorfen-vinphos	470-90-6	0,1	0,1	0,3	0,3	
(9)	Chlorpyrifos (Chlorpyrifos-ethyl)	2921-88-2	0,03	0,03	0,1	0,1	
(9a)	Cyclodiene pesticides: Aldrin (7) Dieldrin (7) Endrin (7) Isodrin (7)	309-00-2 60-57-1 72-20-8 465-73-6	Σ = 0,01	Σ = 0,005	not applicable	not applicable	

(1)	(2)	(3)	(4)	(5)	(6)	(7)	(8)
No	Name of substance	CAS number [1]	AA-EQS [2] Inland surface waters [3]	AA-EQS [2] Other surface waters	MAC-EQS [4] Inland surface waters [3]	MAC-EQS [4] Other surface waters	EQS Biota [12]
(9b)	DDT total [7], [9]	not applicable	0,025	0,025	not applicable	not applicable	
	para-para-DDT [7]	50-29-3	0,01	0,01	not applicable	not applicable	
(10)	1,2-Dichloroe-thane	107-06-2	10	10	not applicable	not applicable	
(11)	Dichlorome-thane	75-09-2	20	20	not applicable	not applicable	
(12)	Di(2-ethylhexyl)-phthalate (DEHP)	117-81-7	1,3	1,3	not applicable	not applicable	
(13)	Diuron	330-54-1	0,2	0,2	1,8	1,8	
(14)	Endosulfan	115-29-7	0,005	0,0005	0,01	0,004	
(15)	Fluoranthene	206-44-0	0,0063	0,0063	0,12	0,12	30
(16)	Hexachloro-benzene	118-74-1			0,05	0,05	10
(17)	Hexachloro-butadiene	87-68-3			0,6	0,6	55
(18)	Hexachloro-cyclohexane	608-73-1	0,02	0,002	0,04	0,02	
(19)	Isoproturon	34123 59 6	0,3	0,3	1,0	1,0	
(20)	Lead and its compounds	7439-92-1	1,2 [13]	1,3	14	14	
(21)	Mercury and its compounds	7439-97-6			0,07	0,07	20
(22)	Naphthalene	91-20-3	2	2	130	130	
(23)	Nickel and its compounds	7440-02-0	4 [13]	8,6	34	34	
(24)	Nonylphenols (4-Nonylphenol)	84852-15-3	0,3	0,3	2,0	2,0	
(25)	Octylphenols ((4-(1,1′,3,3′-tetramethyl-butyl)-phenol))	140-66-9	0,1	0,01	not applicable	not applicable	
(26)	Pentachloro-benzene	608-93-5	0,007	0,0007	not applicable	not applicable	

(1)	(2)	(3)	(4)	(5)	(6)	(7)	(8)
No	Name of substance	CAS number (1)	AA-EQS (2) Inland surface waters (3)	AA-EQS (2) Other surface waters	MAC-EQS (4) Inland surface waters (3)	MAC-EQS (4) Other surface waters	EQS Biota (12)
(27)	Pentachloro-phenol	87-86-5	0,4	0,4	1	1	
(28)	Polyaromatic hydrocarbons (PAH) (11)	not applicable	not applicable	not applicable	not applicable	not applicable	
	Benzo(a)pyrene	50-32-8	$1,7 \times 10^{-4}$	$1,7 \times 10^{-4}$	0,27	0,027	5
	Benzo(b)fluor-anthene	205-99-2	see footnote 11	see footnote 11	0,017	0,017	see footnote 11
	Benzo(k)fluor-anthene	207-08-9	see footnote 11	see footnote 11	0,017	0,017	see footnote 11
	Benzo(g,h,i)-perylene	191-24-2	see footnote 11	see footnote 11	$8,2 \times 10^{-3}$	$8,2 \times 10^{-4}$	see footnote 11
	Indeno(1,2,3-cd)-pyrene	193-39-5	see footnote 11	see footnote 11	not applicable	not applicable	see footnote 11
(29)	Simazine	122-34-9	1	1	4	4	
(29a)	Tetrachloro-ethylene (7)	127-18-4	10	10	not applicable	not applicable	
(29b)	Trichloro-ethylene (7)	79-01-6	10	10	not applicable	not applicable	
(30)	Tributyltin compounds (Tributyltin-cation)	36643-28-4	0,0002	0,0002	0,0015	0,0015	
(30)	Tributyltin compounds (Tributyltin-cation)	36643-28-4	0,0002	0,0002	0,0015	0,0015	
(31)	Trichloro-benzenes	12002-48-1	0,4	0,4	not applicable	not applicable	
(32)	Trichloro-methane	67-66-3	2,5	2,5	not applicable	not applicable	
(33)	Trifluralin	1582-09-8	0,03	0,03	not applicable	not applicable	
(34)	Dicofol	115-32-2	$1,3 \times 10^{-3}$	$3,2 \times 10^{-5}$	not applicable (10)	not applicable (10)	33
(35)	Perfluorooctane sulfonic acid and its derivatives (PFOS)	1763-23-1	$6,5 \times 10^{-4}$	$1,3 \times 10^{-4}$	36	7,2	9,1
(36)	Quinoxyfen	124495-18-7	0,15	0,015	2,7	0,54	

(1)	(2)	(3)	(4)	(5)	(6)	(7)	(8)
No	Name of substance	CAS number (1)	AA-EQS (2) Inland surface waters (3)	AA-EQS (2) Other surface waters	MAC-EQS (4) Inland surface waters (3)	MAC-EQS (4) Other surface waters	EQS Biota (12)
(37)	Dioxins and dioxin-like compounds	See footnote 10 in Annex X to Directive 2000/60/EC			not applicable	not applicable	Sum of PCDD+PCDF+ PCB-DL 0,0065 µg.kg^{-1} TEQ (14)
(38)	Aclonifen	74070-46-5	0,12	0,012	0,12	0,012	
(39)	Bifenox	42576-02-3	0,012	0,0012	0,04	0,004	
(40)	Cybutryne	28159-98-0	0,0025	0,0025	0,016	0,016	
(41)	Cypermethrin	52315-07-8	8×10^{-5}	8×10^{-6}	6×10^{-4}	6×10^{-5}	
(42)	Dichlorvos	62-73-7	6×10^{-4}	6×10^{-5}	7×10^{-4}	7×10^{-5}	
(43)	Hexabromo-cyclododecane (HBCDD)	See footnote 12 in Annex X to Directive 2000/60/EC	0,0016	0,0008	0,5	0,05	167
(44)	Heptachlor and heptachlor epoxide	76-44-8/1024-57-3	2×10^{-7}	1×10^{-8}	3×10^{-4}	3×10^{-5}	$6,7 \times 10^{-3}$
(45)	Terbutryn	886-50-0	0,065	0,0065	0,34	0,034	

(1) CAS: Chemical Abstracts Service.

(2) This parameter is the EQS expressed as an annual average value (AA-EQS). Unless otherwise specified, it applies to the total concentration of all isomers.

(3) Inland surface waters encompass rivers and lakes and related artificial or heavily modified water bodies.

(4) This parameter is the EQS expressed as a maximum allowable concentration (MAC-EQS). Where the MAC-EQS are marked as "not applicable", the AA-EQS values are considered protective against short-term pollution peaks in continuous discharges since they are significantly lower than the values derived on the basis of acute toxicity.

(5) For the group of priority substances covered by brominated diphenylethers (No 5), the EQS refers to the sum of the concentrations of congener numbers 28, 47, 99, 100, 153 and 154.

(6) For Cadmium and its compounds (No 6) the EQS values vary depending on the hardness of the water as specified in five class categories (Class 1: < 40 mg $CaCO_3$/l, Class 2: 40 to < 50 mg $CaCO_3$/l, Class 3: 50 to < 100 mg $CaCO_3$/l, Class 4: 100 to < 200 mg $CaCO_3$/l and Class 5: ≥ 200 mg $CaCO_3$/l).

(7) This substance is not a priority substance but one of the other pollutants for which the EQS are identical to those laid down in the legislation that applied prior to 13 January 2009.

(8) No indicative parameter is provided for this group of substances. The indicative parameter(s) must be defined through the analytical method.

(9) DDT total comprises the sum of the isomers 1,1,1-trichloro-2,2 bis (p-chlorophenyl) ethane (CAS number 50-29-3; EU number 200-024-3); 1,1,1-trichloro-2 (o-chlorophenyl)-2-(p-chlorophenyl) ethane (CAS number 789-02-6; EU Number 212-332-5); 1,1-dichloro-2,2 bis (p-chlorophenyl) ethylene (CAS number 72-55-9; EU Number 200-784-6); and 1,1-dichloro-2,2 bis (p-chlorophenyl) ethane (CAS number 72-54-8; EU Number 200-783-0).

(10) There is insufficient information available to set a MAC-EQS for these substances.

(11) For the group of priority substances of polyaromatic hydrocarbons (PAH) (No 28), the biota EQS and corresponding AA-EQS in water refer to the concentration of benzo(a)pyrene, on the toxicity of which they are based. Benzo(a)pyrene can be considered as a marker for the other PAHs, hence only benzo(a)pyrene needs to be monitored for comparison with the biota EQS or the corresponding AA-EQS in water.

(12) Unless otherwise indicated, the biota EQS relate to fish. An alternative biota taxon, or another matrix, may be monitored instead, as long as the EQS applied provides an equivalent level of protection. For substances numbered 15 (Fluoranthene) and 28 (PAHs), the biota EQS refers to crustaceans and molluscs. For the purpose of assessing chemical status, monitoring of Fluoranthene and PAHs in fish is not appropriate. For substance number 37 (Dioxins and dioxin-like compounds), the biota EQS relates to fish, crustaceans and molluscs, in line with section 5.3 of the Annex to Commission Regulation (EU) No 1259/2011 of 2 December 2011 amending Regulation (EC) No 1881/2006 as regards maximum levels for dioxins, dioxin-like PCBs and non-dioxin-like PCBs in foodstuffs (OJ L 320, 3.12.2011, p. 18).

(13) These EQS refer to bioavailable concentrations of the substances.

(14) PCDD: polychlorinated dibenzo-p-dioxins; PCDF: polychlorinated dibenzofurans; PCB-DL: dioxin-like polychlorinated biphenyls; TEQ: toxic equivalents according to the World Health Organisation 2005 Toxic Equivalence Factors.'